UNIVERSITY OF CALIFORNIA, MERCED

Potential energy surfaces of van der Waals molecules

A Thesis submitted in partial satisfaction of the requirements
for the degree of Master of Science

in

Chemistry

by

Joseph Brent Dizon

Committee in charge:

Professor Erin R. Johnson, Advisor

Professor Michael E. Colvin, Chair

Professor Christine M. Isborn

Professor Kevin A. Mitchell

2014

The Thesis of Joseph Brent Dizon is approved and it is acceptable in quality and form for publication on microfilm and electronically:

Professor Erin Johnson, Advisor

Professor Michael Colvin, Chair

Professor Christine Isborn

Professor Kevin Mitchell

University of California, Merced

2014

DEDICATION

To Mom, Brian, Uncle Gerry, Auntie Au, John B., Gerard, J.P., Uncle Stan, Auntie Cora, Christian, Carlo, and relatives from both in the States and in the Philippines. Thank you for the gift of family and for your support for education and your unconditional love.

To Mrs. Macklin and Mr. Phi. Your teachings and appreciation in chemistry helped me grow to this day and to have fun with chemistry.

To friends at home and at UC Irvine: Garrett, Tri, Truc, Sarah, Bundit, Yuvadee, buddies in the Chemistry House, Mya, Raul, Liwanag, and others. Thank for your support during our time together.

To teachers in Loara High School. You helped me build foundations to relate subjects all together. Mr. Quiroz, you taught math really well, which bridged the connection between math and chemistry. Mr. Pastis, you helped me to relate economics with chemistry.

To Professor Kieron Burke, UC Irvine. Thank you for hooking me to study quantum chemistry and density-functional theory. This journey through chemistry is really unexpected and you made me think like a theoretical and mathematical chemist.

To friends and buddies at UC Merced: Camille, Mandy, David, Cameron, Reza, Calvin, Andrew, Martin, Logan, Diane, Dan, Abe, Christine T., Brandon, Iqbal, Guillermo, Gabe, Nick, Philip, and others. Thank you for your support and dedication during the Merced journey. Ah, those fun times.

To Jon Worrel. Our thoughtful discussions, philosophies, and curiosities were really memorable during the Merced journey. You have philosophies that made me wonder.

LIST OF TABLES

LIST OF FIGURES

CONTENTS

ACKNOWLEDGEMENTS

Special thanks to Dr. Erin Johnson for guiding me throughout this project and providing the opportunity to research in density-functional theory (DFT) with patience, time, and effort. I also thank her for guidance in preparation of this manuscript with helpful discussions and suggestions. I also thank Dr. Alberto Otero-de-la Roza for facilitating this project by enhancing visualizations and figures for the project and setting up programs to carry DFT calculations with Dr. Johnson's exchange-hole dipole moment (XDM) model. I also thank Dr. Otero-de-la Roza and Dr. Johnson for fixing error bugs on the POSTG code, which greatly moved the project forward. In addition, I express my appreciation to my committee: Dr. Johnson, Dr. Christine Isborn, Dr. Michael Colvin, and Dr. Kevin Mitchell. I also thank the Johnson group for providing several helpful suggestions on improving the presentations on the thesis. Thanks to Mark Vidensek of UC Merced for his suggestions of including the rare-gas acetylene van der Waals (vdW) molecule in this project.

ABSTRACT

The potential energy surfaces (PES) of 28 simple rare-gas (Rg)-linear molecule van der Waals (vdW) complexes were calculated using four dispersion-corrected density functionals (HFPBE-XDM, PW86PBE-XDM, a PW86PBE-XDM hybrid functional, and B97-D) and compared with accurate coupled cluster CCSD(T) reference data. In this benchmark study, the quality of the PES are assessed based on the values of the binding energies (BEs), and the geometry at the global minimum and the overall anisotropies and shapes of the PES. All functionals perform adequately on Rg-H_2, Rg-N_2, Rg-CO, Rg-OCS, and Rg-CO_2 dimers. The functionals display various problems for the remaining vdW molecules. In particular, B97-D predicts overbound global minima and incorrect geometries for He,Ne,Ar,Kr-HCN and Ne,Ar,Kr-C_2H_2, PW86PBE-XDM and the hybrid functional massively overbind Rg-HF, and HFPBE-XDM predicts different global minima than the reference PES for Rg-HCl and Rg-HBr complexes. The error trends of the functionals are assessed relative to the size of the Rg atoms and the polarity of the linear molecules. Based on this assessment, we find that delocalization error affects the performance of the functionals and depends on the polarity of the linear molecule. The hybrid functional, which we denote as PW1PBE-XDM, provides lower error statistics than other functionals, which leads to a possibility that this functional can be applied to study other classes of vdW molecules in future PES studies.

I. INTRODUCTION

The calculation of weak van der Waals (vdW) interactions is a challenging task with applications in chemistry, physics, and biology. Much in this area of research concentrates on developing accurate treatments of vdW interactions that exist between noncovalently-bonded, closed-shell molecules called vdW molecules. vdW molecules are bound by a balance between long-range and short-range contributions to the overall vdW interaction[1–3]. Long-range interactions include electrostatic interactions, which arise from the interaction between the permanent charge distributions of the two monomers (i.e. atoms or molecules); induction, which comes from the distortion of the monomer charge distribution in response to the electric field of the other monomer's electrons; and dispersion, which arises due to instantaneous fluctuations in the charge distribution of each monomer. Short-range interactions are also present due to the overlap of the wavefunctions between monomers. The most dominant short-range contribution is exchange-repulsion, which is responsible for the repulsion of electrons as the monomers come into close contact. The overall vdW interaction energy is attractive where the long-range electrostatic, induction, and dispersion contributions are negative, while the short-range exchange-repulsion contributions are positive. In general, the vdW interaction is a dynamical correlation effect[4] that arises due to the many-body effects between electrons in the monomers. However, dispersion is more difficult to describe accurately than the other contributions since dispersion arises from very long-range electron correlation due to instantaneous interactions between electrons on different centers[4,5]. In this context, the movement of electrons depends on the presence of other electrons. Thus, dispersion is a non-local dynamical correlation effect[4]. Treating dispersion accurately is tremendously essential because the structures of many systems of interest are determined, in part, by dispersion, including bioorganic molecules, molecular crystals, surface adsorption, and gas-phase molecular dimers[1,5].

Many studies of vdW molecules aimed to describe the full vdW interaction in terms of the potential energy surface (PES). The PES maps the vdW interaction in terms of interaction energies dependent on the relative orientation and distance of the two monomers[2,3,6–8]. Jacobi coordinates are used to generate the configuration space of the PES[3]. For instance, the PES of a prototypical rare-gas (Rg)-linear molecule vdW dimer contains two degrees of freedom: the bond distance from the Rg atom to the center-of-mass of the linear molecule (normally denoted as R) and the bond angle between the axis of the linear molecule, the center of mass, and the Rg atom (denoted as θ)[8]. The bond lengths of the linear molecule are generally fixed to reduce the number of degrees of freedom of the PES. The PES describes the orientation-dependent behavior of the vdW interaction and locates the most stable geometry of the vdW molecule in terms of the lowest energy (global minimum) and other competing structures (local minima, if any). Moreover, the PES provides useful information to describe the dynamics of vdW molecules in terms of rovibrational spectra and bound states[2,3,6,8]. In short, the PES is mainly used to reveal the structure and dynamics of vdW molecules.

FIG. 1. Jacobi coordinates for the Rg-hydrogen halide complex.

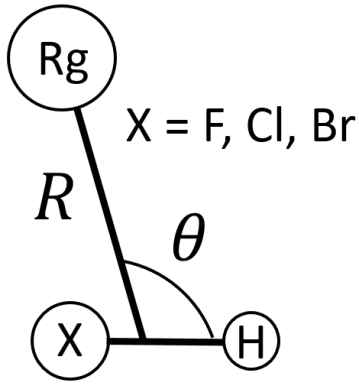

Experimental and computed PES of Rg-linear vdW molecules have been constructed thoroughly and are well-known in the literature[2,3,6–8]. Advances in spectroscopy (both experimental technology and theory)[6,7,9] have made the determina-

tion of highly-accurate PES possible, leading to predictions of the lowest energy configurations, presence of other bound states, rovibrational spectra, and dynamics of Rg-linear complexes[3,6,8]. Analytical PES can be carefully fitted to experimental data and account for long-range and short-range vdW interactions by using asymptotic expansions[6,8]. In addition, experimental PES account for molecular vibrations of the linear molecules and intermolecular nuclear motions, which are essential to describe the spectra accurately. A more complete description of the vdW interaction involves the vibrational average of the PES from the ground state and the first excited state since vdW molecules are not always present in their ground state[8]. Overall, the PES predicts spectroscopic information for Rg-linear molecule vdW complexes, which can be verified experimentally[6,8,9].

Computational studies of vdW molecules are carried out to verify experimental results and to predict the shape of the PES when experimental data are not available. Methods of calculating the PES use a supermolecule approach to calculate interaction energies, or binding energies (BEs), by taking the difference between the energy of the vdW dimer and the energies of each monomer[2,3,8]. As a first approximation, computational methods treat the linear molecule as a rigid rotor and the nuclear motions between the Rg atom and the linear molecule are frozen. This simplifies the calculation of the PES and yields reasonable BEs, lowest-energy configurations, and correct anisotropies. A rigid-rotor approximated PES may provide accurate spectroscopic data that agrees with experiment. However, the calculation of the PES requires appropriate measures such as the selection of a large-enough basis set[3,8], removal of basis-set-superposition-error (BSSE)[2,3,8] with counterpoise-correction (CP) methods[10], and the inclusion of dispersion. BSSE arises due to the large energy difference between the energy of the dimers and monomers in a given basis set[3]. For a given basis set of a dimer, the basis functions of each monomer compensates for the basis set incompleteness of the other monomer[11]. Consequently, the BEs becomes largely overbound[3,11]. CP correction methods are designed to remove the BSSE to compute BEs[3]. Self-consistent field (SCF) calculations[2,3], which are done

in an iterative procedure such as Hartree-Fock (HF) theory, have difficulties treating dispersion since they do not take into account electron correlation appropriately. Post-SCF methods were developed to tackle the shortcomings of SCF methods. Methods such as configuration interaction (CI)[12], Møller-Plesset (MP) perturbation theory[3,13], and coupled-cluster methods[14] provide various degrees of dynamical correlation, which account for the vdW interaction. There are known deficiencies for several post-SCF methods. CI is not size consistent since the sum of the energies of the dimer at infinite separations is different from the individual sum of the monomer energies when computed separately[3,12]. MP perturbation theory is also problematic since the perturbation series may not converge[3,15]. Moreover, both CI and MP perturbation theory are affected by BSSE due to the finite size of the basis set[3]. A complete and correct description of dispersion requires inclusion of electron correlation using coupled-cluster methods[16] or symmetry-adapted perturbation theory (SAPT)[9,17–19]. However, conventional density-functional theory (DFT) methods are not accurate for modeling dispersion unless non-local effects are included[19]. Consequences are severe when dispersion energies are incorrectly calculated, such as predicting unbound complexes and repulsive or artificially low BEs, and incorrect anisotropies and shapes of the PES.

In recent years, researchers[8] employed coupled-cluster methods to calculate highly accurate PES for Rg-linear complexes that reproduce experimental PES. The popular CCSD(T) method (the coupled cluster single and double excitations with a non-iterative perturbation treatment of triple excitations)[14] reproduces appropriate behavior of the PES at both short and long-range. Authors employ CCSD(T) calculations with large basis sets including midbond functions to speed the convergence of computed BEs[8]. In addition, several authors treat the linear molecule as a rigid rotor and others account for vibrational motions of the linear molecule by including vibrational coordinates in addition to traditional Jacobi coordinates. They claimed that the rigid-rotor model may not be sufficient to compute accurate spectra beyond the ground state since intermolecular vibrations were neglected[8]. Thus some of the PES

are vibrationally averaged to account for intermolecular vibrations[8]. The PES are also used to determine the most stable, lowest-energy configurations of the vdW complex and its rovibrational properties[2,3,8,9]. The construction of the PES with CCSD(T) is computationally demanding and it is impractical for larger systems. Despite its computational expense, CCSD(T) is a popular source of reference data to compare and assess the overall performance of other promising computational methods for PES and for BEs of vdW molecules that include simple biological and organic molecules and exhibit various types of intermolecular forces. CCSD(T) is an appropriate standard for benchmarking studies.

Density-functional theory (DFT) methods have gained tremendous attention in recent years for treatment of vdW interactions[5,20,21]. In DFT, the energy is expressed as a functional of the density[20,21]. DFT is widely used in computational chemistry because it performs well for thermochemistry with low computational cost[20,21]. However, popular conventional functionals such as the local density approximation (LDA) and generalized gradient approximation (GGA) have serious drawbacks for describing dispersion[22]. First, contributions to the exchange-correlation energy arise only in overlapping regions of the monomer electron densities, whereas the dispersion energy remains significant in cases where the monomer densities are non-overlapping[5,23]. Second, the long-range decay behavior of the PES, particularly with GGAs, has an exponential decay rather than the correct $-1/R^6$ behavior, which is a main characteristic of the dispersion energy[24]. Problems with these functionals were revealed from computational studies of Rg dimers, where functionals either predicted the interaction between the Rg dimers to be significantly overbound or underbound depending on the functional[22,25]. Since vdW interactions arise from dynamical correlation effects (both local and non-local)[4,5], conventional functionals have difficulties in describing these interactions particularly the highly non-local dynamical correlation effects that give rise to dispersion.

Dispersion-corrected methods were proposed to tackle the shortcomings of semilocal functionals for vdW complexes[5,20,21]. One of these approaches is fitting the func-

tionals to reproduce BEs of vdW molecules, a popular approach used in the development of the Minnesota functionals by Truhlar and coworkers[5,20,21,26,27]. This allows functionals to predict accurate BEs at the minimum conformation. The problem is that these functionals are not designed to include the correct asymptotic behavior, even though they can be used to obtain useful equilibrium properties. Another approach is to include a simple pair-wise additive -C_6/R^6 correction term that is added to the total DFT energy[5,28]. This approach computes dispersion energies with an affordable computational cost. To remove the divergence of the dispersion-correction term at short-range, a damping function is used[5,28]. One of the popular functionals that incorporates this approach is the B97-D functional[29]. The dispersion coefficients are computed from the London dispersion formula, using ionization potentials and static dipole polarizabilities from DFT calculations. The dispersion-correction term includes a global scaling parameter that is compatible with the B97 functional[30]. The B97-D functional is constructed from adjusting the short-range portion of the B97 hybrid GGA functional in the presence of the long-range correction term. As a result, B97-D obtains accurate heats of formation for the G97/2 test set[31] and it performs well for the vdW molecules within the training set. Other functional developments emphasize dispersion coefficients that depend on the chemical environment. For instance, Becke and Johnson developed a method to calculate nonempirical dispersion coefficients that depend on dipole moments of the exchange hole, atomic polarizabilities, effective volumes, and expectation values of the multipole operators. This is the basis of the exchange-hole dipole moment (XDM) model that expresses the dispersion energy as a functional of the density and orbitals.

Despite of the relative successes of conventional functionals for predicting properties of atoms, molecules, and solids and dispersion-corrected functionals for describing vdW interactions, these functionals suffer from systematic errors, one of which is the delocalization error[5,20,21,32]. Delocalization error is a well-known systematic error where functionals predict non-physical properties[5,20,32]. Delocalization error leads to the following major consequences: underestimation of reaction barriers of

chemical reactions, band gaps of materials, the energies of dissociating molecular ions, and charge-transfer excitation energies and the overestimation of BEs of charge-transfer complexes and response properties of molecules and materials to an electric field[32]. A classic example of delocalization error is the dissociation energy curve of the H_2^+ molecule[20,21,24,32]. The BEs at the minimum and the short-range repulsion are reasonable, but when the H atoms are separated at long-range, the BE becomes increasingly negative as a result of the delocalization of charge between the two H atoms. Consequently, each H atom has a fractional charge, which causes incorrect stability at large separations. Due to the possible formation of fractional charges on each monomer, this non-physical overstabilizing behavior can occur in highly-polar vdW or charge-transfer complexes when modeled with GGAs due to the sensitivity of GGAs to delocalization error. To reduce delocalization error, range-separated functionals, which include a long-range exact exchange term and a short-range term that uses a density-functional approximation, are commonly used[5,20,21]. Other approaches combine exact (Hartree-Fock) exchange with non-local correlation functionals to describe dispersion, which is advantageous in taking account of dispersion at long-range. However, using fully non-local functionals increases the computational cost. Functional development is tricky since increasing the level of theory, as with non-local functionals, does not always guarantee improved accuracy, while less-sophisticated functionals are less computationally expensive, but susceptible to delocalization error. Functional development is still in progress to tackle the delocalization error problem and to enhance the description of dispersion between vdW molecules[5,20].

In this work, we computed PES using the exchange-hole dipole moment (XDM) dispersion model by Becke and Johnson[33–39]. XDM has the necessary components to calculate nonempirical dispersion coefficients and it describes the proper physics of the dispersion interaction. The idea is that dispersion-corrected functionals can be used with any number of base functionals that recover correct exchange-repulsion behavior similar to HF, but we must also consider delocalization error. We chose a combination of base exchange and correlation functionals paired with XDM. We include the

HFPBE-XDM functional, which pairs non-local HF exchange with a semilocal GGA correlation functional, to explore the effects of the full treatment of exact exchange. We also select PW86PBE-XDM, a GGA functional that includes PW86 exchange, which reproduces the HF exchange-repulsion at short-range in PES of Rg dimers[40], and PBE correlation. PW86PBE-XDM performs excellently for the Kannemann-Becke set of 65 molecules (KB65) and for the Rg dimer set[40], which justifies our selection of this functional. Finally, we selected a new PW86PBE-XDM hybrid functional (denoted as the PW1PBE-XDM) that includes a fraction of exact exchange and a portion of GGA exchange, paired with GGA correlation. The inclusion of the hybrid may improve the overall performance for the PES by including additional non-local effects from exact exchange. In addition, we will compare XDM-corrected functionals to the popular empirical B97-D functional since the ability of the latter method to give accurate PES has not yet been studied in the literature. Density-functional treatments of the PES are known. For instance, density-functionals with a mixture of exact exchange were paired with damped dispersion corrections[41–43]. Other approaches combined the long-range correction scheme for exact exchange with the Andersson-Langreth-Lundqvist (ALL)[44] vdW functional to obtain accurate PES of Rg dimers[45] and other Rg-linear molecule vdW complexes[46]. Alternatively, double hybrid functionals[47] were implemented to obtain satisfactory PES of various Rg-linear molecules[48,49].

One of the goals of this work is also to assemble a benchmark set to assess the performance of the functionals compared with accurate reference data. The benchmark set of Rg-linear dimers is an appropriate and extremely sensitive test for base-XDM functionals and B97-D. The comparison between CCSD(T) and dispersion-corrected DFT methods is appropriate because both methods account for dispersion via non-local dynamical correlation. The set includes complexes of noble gas atoms and linear molecules of varying size (size of the atoms and the number of atoms) and polarity. The following linear molecules are chosen to pair with the Rg atoms: nonpolar molecules (H_2, N_2, CO_2, and C_2H_2), moderately polar molecules (CO, OCS, HCl,

and HBr), and highly-polar molecules (HF and HCN). This set of vdW molecules includes various intermolecular forces, including dispersion and dipole-induced dipole interactions between the Rg atom and the linear molecule. Twenty-eight Rg-linear molecule complexes are selected depending on the availability of CCSD(T) reference PES and BE data. The list of molecules is shown in Tables I-III, which include BEs and optimized geometries for the global minimum of each dimer. In this work, we briefly outline the XDM method, the base functionals, and implementation in Sec.II. Sec.III highlights the overall performance of base-XDM functionals based on qualitatively comparing the PES and quantitatively comparing the BEs and geometries at the global minimum to CCSD(T) reference data. Finally, we conclude by selecting the functional which gives the most accurate PES.

II. THEORY

A. The exchange-hole dipole moment model

The exchange-hole dipole moment (XDM) model is a method by Becke and Johnson[33–39] that describes dispersion interactions from the dipole moment of the exchange-hole. For a given electron of σ spin at $\boldsymbol{r}_1$, which is the reference point in an atom or a molecule, the exchange-hole $h_{X\sigma}(\boldsymbol{r}_1,\boldsymbol{r}_2)$ measures the depletion of probability, with respect of the total electron density ρ_σ, to find another electron at $\boldsymbol{r}_2$ with the same spin. The hole is expressed as pair-wise sum over occupied orbitals, which can be Kohn-Sham or Hartree-Fock orbitals[33]

$$h_{X\sigma}(\boldsymbol{r}_1,\boldsymbol{r}_2) = -\frac{1}{\rho_\sigma(\boldsymbol{r}_1)}\sum_{ij}\psi_{i\sigma}(\boldsymbol{r}_1)\psi_{j\sigma}(\boldsymbol{r}_1)\psi_{i\sigma}(\boldsymbol{r}_2)\psi_{j\sigma}(\boldsymbol{r}_2). \tag{1}$$

The features of the exact hole include the following conditions[33,50]: The probability of finding another electron at $\boldsymbol{r}_1 = \boldsymbol{r}_2$ is extinguished completely as required by the Pauli Principle

$$h_{X\sigma}(\boldsymbol{r}_1,\boldsymbol{r}_1) = -\rho_\sigma(\boldsymbol{r}_1), \tag{2}$$

the hole is always negative $h_{X\sigma}(\boldsymbol{r}_1,\boldsymbol{r}_2) < 0$, and the hole will always normalized to one electron

$$\int h_{X\sigma}(\boldsymbol{r}_1,\boldsymbol{r}_1) = -1. \tag{3}$$

The hole is usually asymmetric around the reference point $\boldsymbol{r}_1$. Therefore, a nonzero dipole moment is present even though the overall charge between the hole and the electron is zero. The dipole moment upon integrating Eq. (1) with respect of $\boldsymbol{r}_2$ is[33]

$$\boldsymbol{d}_{X\sigma}(\boldsymbol{r}_1) = \left[\frac{1}{\rho_\sigma(\boldsymbol{r}_1)}\sum_{ij}\boldsymbol{r}_{ij\sigma}\psi_{i\sigma}(\boldsymbol{r}_1)\psi_{j\sigma}(\boldsymbol{r}_1)\right] - \boldsymbol{r}_1 \tag{4}$$

$$\boldsymbol{r}_{ij\sigma} = \int \boldsymbol{r}_2 \psi_{i\sigma}(\boldsymbol{r}_2)\psi_{j\sigma}(\boldsymbol{r}_2) d^3\boldsymbol{r}_2.$$

The dipole moment of the exchange hole from Eq. 4 is position dependent and is generally non-zero. This expression is a key ingredient to derive the dispersion energy.

The hole can be Taylor expanded to second order near the reference point, where the hole is written as a spherical average of of $h_{X\sigma}(\boldsymbol{r}_1,\boldsymbol{r}_2)$ around $\boldsymbol{r}_1$[35]

$$h_{X\sigma}(\boldsymbol{r}, \boldsymbol{r}+s) = -\rho_\sigma - Q_\sigma s^2 \tag{5}$$

where s is the interelectronic distance, and

$$Q_\sigma = \frac{1}{6}\left[\nabla^2\rho_\sigma - 2\tau_\sigma + \frac{1}{2}\frac{(\nabla\rho_\sigma)^2}{\rho_\sigma}\right] \tag{6}$$

where the kinetic energy density τ_σ is

$$\tau_\sigma = \sum_i (\nabla\psi_{i\sigma})^2. \tag{7}$$

Eqs 5-7 are the components of the Becke-Roussel (BR) model[51], which approximates the behavior of the exact exchange hole. Since the exchange-hole from Eq. 1 is exact, involving a sum over occupied orbitals, the computational cost increases significantly for larger systems such as solids. Thus, an approximation to the exact hole is appropriate to reduce computational cost[35].

The construction of the BR hole[35] uses an off-centered exponential $(a^3/8\pi)e^{-ar}$ at a distance b from the reference point. The hole is derived from the density of the hydrogen atom and it is computed by taking a spherical average centered at the reference point. The hole is expressed in terms of a and b and the hole is normalized. The derivatives of the BR hole are taken at the reference point to equate the coefficients of the second-order Taylor expansion form of the exchange-hole from Eq. 5 to obtain the correct curvature at the reference point. The resulting non-linear equation[35], which is numerically solvable, is

$$\frac{xe^{-2x/3}}{x-2} = \frac{2}{3}\pi^{2/3}\frac{\rho_\sigma^{5/3}}{Q_\sigma}. \tag{8}$$

The value of x is numerically solved and, by using the relation $x = ab$, the resulting expression for b is

$$b^3 = \frac{x^3 e^{-x}}{8\pi\rho_\sigma}, \tag{9}$$

which obtains the correct values of a and b. The BR hole depends on ρ_σ, $\nabla\rho_\sigma$, $\nabla^2\rho_\sigma$, and τ_σ, which are the components of a meta-GGA functional.

Since the exchange-hole has a non-zero dipole moment, higher-order multipole moments are also present[36,38]. As an example, for a simple spherical atom, the exchange-hole dipole moment faces towards the nucleus. For an electron a distance r from the nucleus, the distance between the mean position of the hole to the nucleus at the origin is $(r - d_{X\sigma})$. At the nucleus, there are higher multipole moments that exist in addition to non-zero dipole moments. The l-multipole moment can be written as[36,38]

$$M_{l\sigma} = -[r^l - (r - d_{X\sigma})^l], \tag{10}$$

which is dependent only on the magnitude of $d_{X\sigma}$. This is an important feature of the XDM model because the magnitude of the exchange-dipole moment can be approximated by using the BR exchange-hole model through densities alone[35]. The magnitude of the dipole moment is

$$d_{X\sigma}(\boldsymbol{r}) = b. \tag{11}$$

Becke and Johnson derived an approach[36,38] to describe the dispersion interaction by using the spherical interaction model. From their simple model of two monomers, there is an interaction potential that includes multiple moments of the electron plus the hole at position $\boldsymbol{r}_A$ in monomer A interacting with the multiple moments of the electron plus the hole at position $\boldsymbol{r}_B$ in monomer B. Second-order perturbation theory was used to compute the dispersion energy to obtain dispersion coefficients

that depend on the multipole moments and atomic polarizabilities by squaring the interaction potential, integrating the interaction for all positions $\boldsymbol{r}_A$ and $\boldsymbol{r}_B$, and dividing by the average excitation energy[36,38].

A further feature of XDM[34,38] involves the partitioning of a molecular system into atoms using the Hirshfeld partitioning scheme[52] where the weight for an atom i is

$$w_i(\boldsymbol{r}) = \frac{\rho_i^{\mathrm{at}}(\boldsymbol{r})}{\sum_m \rho_m^{\mathrm{at}}(\boldsymbol{r})} \tag{12}$$

where ρ^{at} is a spherical, free-atomic density placed at the appropriate nucleus and the m summation runs over all nuclei. At the vicinity of nucleus i, $w_i(\boldsymbol{r})$ is 1 while it will approach 0 far from that atom. The sum of the weights will equal 1 at each grid point. The partitioning scheme decomposes the density into atomic pieces. By incorporating the partition scheme, the expectation value of the multipole moment becomes[36,38]

$$\langle M_l^2 \rangle_i = \sum_\sigma \int w_i(\boldsymbol{r}) \rho_\sigma(\boldsymbol{r}) [r_i^l - (r_i - d_{X\sigma})^l]^2 d^3\boldsymbol{r}. \tag{13}$$

The average excitation energy, which is computed from second-order perturbation theory, is related to the atomic polarizability, which is the tendency for an atom to respond to a perturbation of the electric field. By applying the partition scheme, it can be generalized that an effective polarizability α_i can be written based on a qualitative relationship between polarizability and volume[36,38]

$$\alpha_i = \frac{\langle r^3 \rangle_i}{\langle r^3 \rangle_{i,free}} \alpha_{i,free} \tag{14}$$

where the following integrals $\langle r^3 \rangle_i$ and $\langle r^3 \rangle_{i,free}$ are

$$\langle r^3 \rangle_i = \int r^3 w_i(\boldsymbol{r}) \rho(\boldsymbol{r}) d^3\boldsymbol{r} \tag{15}$$

and

$$\langle r^3 \rangle_{i,free} = \int r^3 \rho_{i,free}(\boldsymbol{r}) d^3\boldsymbol{r} \tag{16}$$

for atomic index i.

The dispersion energy is generally written as an asymptotic series[33–37]

$$E_{disp} = -\sum_{n=6,8,10} \sum_{ij} \frac{C_{n,ij}}{R_{ij}^n} \tag{17}$$

where R_{ij} is the distance between the nuclei and this series diverges for small R_{ij}. One way to remove the divergence of the dispersion energy is to use a damping function proposed by Becke and Johnson[37,38],

$$f(R_{ij}) = \frac{R_{ij}^n}{R_{vdw,ij}^n + R_{c,ij}} \tag{18}$$

where $R_{c,ij}$ is the critical distance that takes the average of the ratio of dispersion coefficients[37,38]

$$R_{c,ij} = \frac{1}{3}\left[\left(\frac{C_{8,ij}}{C_{6,ij}}\right)^{1/2} + \left(\frac{C_{10,ij}}{C_{6,ij}}\right)^{1/4} + \left(\frac{C_{10,ij}}{C_{8,ij}}\right)^{1/2}\right], \tag{19}$$

and $R_{vdw,ij}$ is the effective vdW separation that has two universal fit parameters a_1 and a_2

$$R_{vdw,ij} = a_1 R_{c,ij} + a_2. \tag{20}$$

The selection of parameters a_1 and a_2 will depend on the choice of exchange and correlation functionals as described in Sec.II B and Sec.II C. Combining all the equations together, the XDM dispersion energy[38,39] is

$$E_{disp}^{\mathrm{XDM}} = -\sum_{n=6,8,10} \sum_{ij} \frac{C_{n,ij}}{R_{vdw,ij}^n + R_{c,ij}^n} \tag{21}$$

and the dispersion coefficients are[37,38]

$$C_{6,ij} = \frac{\alpha_i \alpha_j \langle M_1^2 \rangle_i \langle M_1^2 \rangle_j}{\langle M_1^2 \rangle_i \alpha_j + \langle M_1^2 \rangle_j \alpha_i} \tag{22}$$

$$C_{8,ij} = \frac{3}{2}\frac{\alpha_i\alpha_j\left(\langle M_1^2\rangle_i\langle M_2^2\rangle_j + \langle M_2^2\rangle_i\langle M_1^2\rangle_j\right)}{\langle M_1^2\rangle_i\alpha_j + \langle M_1^2\rangle_j\alpha_i} \tag{23}$$

$$C_{10,ij} = 2\frac{\alpha_i\alpha_j\left(\langle M_1^2\rangle_i\langle M_3^2\rangle_j + \langle M_3^2\rangle_i\langle M_1^2\rangle_j\right)}{\langle M_1^2\rangle_i\alpha_j + \langle M_1^2\rangle_j\alpha_i} + \frac{21}{5}\frac{\alpha_i\alpha_j\langle M_2^2\rangle_i\langle M_2^2\rangle_j}{\langle M_1^2\rangle_i\alpha_j + \langle M_1^2\rangle_j\alpha_i}. \tag{24}$$

The main advantage of XDM is that the dispersion energy can be computed after performing a DFT calculation with a corresponding base functional. XDM is nonempirical and fast, thus it is physically meaningful to treat dispersion and efficient[5,21,38,39].

B. DFT and exchange-correlation functionals

The basic machinery of DFT is the total energy functional that depends on the electron density rather than a wavefunction[53]. The formulation of Hohenberg-Kohn theorems[54] and Kohn-Sham equations[55] made DFT applicable to physical, chemical, and biological problems due to the key ingredient of the total DFT energy: the exchange-correlation energy. The total energy is[20,21,23,53,55]

$$E[\rho] = T_s[\rho] + V_{ne}[\rho] + J[\rho] + E_{xc}[\rho] \tag{25}$$

where $T_s[\rho]$ is the non-interacting kinetic energy, $V_{ne}[\rho]$ is the electron-nuclear attraction energy, $J[\rho]$ is the self-repulsion energy, $E_{xc}[\rho]$ is the exchange-correlation energy, and the electron density is

$$\rho_\sigma(\boldsymbol{r}) = \sum_i |\psi_{i\sigma}(\boldsymbol{r})|^2 \tag{26}$$

where $\psi_{i\sigma}(\boldsymbol{r})$ is a single-particle Kohn-Sham orbital. The energies are obtained by solving the Kohn-Sham equations self-consistently[20,21,53,55]. Expressions for the non-interacting kinetic energy, electron-nuclear attraction energy, and the self-repulsion energy are known, but the exact functional form for the exchange-correlation energy

is unknown[20,21,53]. An appropriate approach to approximate the exchange-correlation energy is to split $E_{xc}[\rho]$ into exchange $E_x[\rho]$ and correlation $E_c[\rho]$ functionals[23,53]

$$E_{xc}[\rho] = E_x[\rho] + E_c[\rho] = \int d^3\boldsymbol{r}\rho(\boldsymbol{r})\epsilon_x + \int d^3\boldsymbol{r}\rho(\boldsymbol{r})\epsilon_c \tag{27}$$

where ϵ_x and ϵ_c are the exchange and correlation energy densities per particle, respectively. Exchange arises due to the repulsion of electrons with the same spin; a consequence of the Pauli-exclusion principle[21]. The correlation energy takes care of other many-body correlation effects and it arises from the cusp conditions of the electron density[4]. The exchange-correlation energy, which is a small portion of the overall DFT energy, contributes to the binding nature of atoms and molecules due to the non-random and correlated motion of electrons[24]. Moreover, the exchange-correlation functional is also designed to correct the non-interacting kinetic energy and the self-repulsion energy, which makes DFT a promising area of research to obtain accurate exchange-correlation energies for noncovalent systems[20]. In general, both the exchange and correlation energies are negative and the exchange energy makes up the majority of the exchange-correlation energy[23,53]. The exact form of exchange is known, which is Hartree-Fock (HF) exchange[21]. In contrast, correlation functionals are less obvious to construct[21]. Many approximate exchange and correlation functionals are constructed to satisfy properties of the exchange and correlation holes, respectively.

One of the earliest approximations to the exchange-correlation energy is the local density approximation (LDA). The LDA energy depends on the local density alone and its derivation is based on the properties of the uniform electron gas[20,21,23,53]. The exchange functional of the LDA is

$$E_x^{\mathrm{LDA}}[\rho] = \int d^3\boldsymbol{r}\rho(\boldsymbol{r})\epsilon_x^{\mathrm{unif}}(\rho(\boldsymbol{r})) = C_x \int d^3\boldsymbol{r}\rho(\boldsymbol{r})^{4/3} \tag{28}$$

where $\epsilon_x^{\mathrm{unif}}(\rho) = C_x\rho(\boldsymbol{r})^{1/3}$ is the exchange energy density per particle for the uniform electron gas and C_x = -3/4$(3/\pi)^{1/3}$. The correlation functional for LDA was

obtained by parameterization to values from quantum Monte Carlo calculations[53,56]. The LDA performs well for systems with uniform density or extremely slowly-varying densities, such as simple metals[53]. For spin-polarized systems, the spin variant of LDA is used, which is the local-spin density-approximation (LSDA)[23,53]. The LDA (or LSDA) perform well for molecular geometries, dipole moments, and vibrational frequencies, but molecules are massively overbound. However, molecules and atoms do not have uniform or slowly-varying densities, thus corrections to the LDA (or LSDA) are necessary to account for changes in the density that will describe correct properties of atoms and molecules.

The construction of exchange functionals comes from exploiting and reproducing the properties of the exact exchange hole from Sec.II A. One of the earliest approaches to account for changes in the electron density is the gradient expansion, which includes the gradient of the density, $\nabla\rho$, its second derivative or the Laplacian, $\nabla^2\rho$, and its higher order derivatives[21,23]. However, the gradient expansion is not effective since it violates properties of the exchange hole and the results were less encouraging than LDA (or LSDA)[21,23]. The generalized gradient approximation (GGA) was designed to correct the deficiencies of LDA (or LSDA) and the gradient expansion by satisfying properties of the exact exchange hole[20,21,50,53]. GGAs are local. Meta-GGAs, which depend on τ, are semi-local[50]. The exchange-correlation functional for GGAs is also expressed in terms of separate exchange and correlation terms. Popular GGA exchange functionals that became useful in chemistry are Perdew-Wang-86 (PW86)[57], Becke-88 (B88)[58], Perdew-Wang-91 (PW91)[59], and Perdew-Burke-Ernzerhof-96 (PBE)[60] exchange.

A general form of the GGA exchange energy functional is[53]

$$E_x^{\mathrm{GGA}}[\rho] = \int d^3\boldsymbol{r}\rho(\boldsymbol{r})\epsilon_x^{\mathrm{GGA}}(\rho(\boldsymbol{r}), \nabla\rho(\boldsymbol{r})) = C_x \int d^3\boldsymbol{r}\rho(\boldsymbol{r})^{4/3}F(s) \tag{29}$$

where $\epsilon_x^{\mathrm{GGA}}(\rho, \nabla\rho)$ is the exchange energy density per particle, which is also written as $\epsilon_x^{\mathrm{unif}}(\rho)F(s)$, and $F(s)$ is an expression that includes the reduced density gradient

$$s = \frac{|\nabla\rho|}{2k_F\rho} \tag{30}$$

where $k_F = (3\pi^2\rho)^{1/3}$ is the Fermi wave vector. The main characteristic of GGA functionals is that they include dependence on the density ρ and its gradient, $\nabla\rho$. GGA functionals recover LDA exchange when $F(s) = 1$, and for non-uniform densities, LDA exchange is corrected by finding an appropriate function $F(s)$ that will retain the known properties of the hole[50]. Perdew and Wang proposed a GGA exchange functional[57] with

$$F(s) = (1 + 1.296s^2 + 14s^4 + 0.2s^6)^{1/15}. \tag{31}$$

This PW86 functional was originally designed to correct the gradient expansion with real-space cutoffs. PW86 exchange is non-empirical since the parameters are determined from fitting the exact exchange hole[57]. In addition, PW86 exchange reproduces quite well the exchange part of the long-range interaction between Rg atoms[50,61] due to the $s^{2/5}$ term in $F(s)$[39]. Thus, this functional is suitable to pair with XDM. Even though PW86 and XDM borrow from the same roots by satisfying some properties of the exact hole, an appropriate correlation functional is necessary to complement the exchange functionals.

GGA correlation functionals are constructed from satisfying various conditions of the correlation hole[62], and one of the main constraints is the sum rule where the integration of the density of the correlation hole is zero[50]. Functionals that were constructed by using specific conditions are Lee-Yang-Parr (LYP) correlation[63], PW91 correlation[64], Perdew-Burke-Ernzerhof (PBE) correlation functional[60], and many others[20,21]. PBE is a GGA functional that incorporates the properties of LSDA, the sum rule of the correlation hole, and fundamental constants as parameters, which is a simplification of the PW91 correlation functional. The PBE correlation functional has the form[23,60,62]

$$E_c^{\mathrm{PBE}} = \int d^3\boldsymbol{r}\rho(\boldsymbol{r})\{\epsilon_c(r_s,\zeta) + H^{\mathrm{PBE}}(r_s,\zeta,t)\} \tag{32}$$

where r_s is the Seitz radius

$$r_s = (3/4\pi\rho)^{1/3}, \tag{33}$$

ζ is the relative spin polarization to account for uneven electron-spin densities

$$\zeta = \frac{(\rho_\uparrow - \rho\downarrow)}{\rho}, \tag{34}$$

t is the reduced density gradient, related to the Thomas-Fermi screening wavevector k_s

$$t = \frac{|\nabla\rho|}{2k_s\phi\rho}, \tag{35}$$

$$k_s = (4k_F/\pi)^{1/2}, \tag{36}$$

ϕ is the spin-scaling factor

$$\phi = \frac{1}{2}[(1+\zeta)^{2/3} + (1-\zeta)^{2/3}], \tag{37}$$

and H^{PBE} is the enhancement factor

$$H^{\mathrm{PBE}} = \gamma\phi^3 \ln\left(1 + \frac{\beta}{\gamma}t^2\left[\frac{1+At^2}{1+At^2+A^2t^4}\right]\right) \tag{38}$$

where

$$A = \frac{\beta}{\gamma}[\exp\{-\epsilon_c^{\mathrm{unif}}/\gamma\phi^3\} - 1]^{-1}, \tag{39}$$

and the constants are $\gamma = 0.031091$ and $\beta = 0.066725$. This functional was developed from satisfying slowly-varying, high-varying, and high-density limits and uniform-scaling conditions. Thus, the PBE correlation functional is nonempirical[60,62].

Combining the XDM dispersion energy, the PW86 exchange, and the PBE correlation functionals gives an approximated E_{xc}

$$E_{xc}^{\mathrm{PW86PBE}} = E_x^{\mathrm{PW86}} + E_c^{\mathrm{PBE}} + E_{disp}^{\mathrm{XDM}}. \tag{40}$$

The PW86PBE-XDM functional performs well for the Rg gas dimer set[40] and the KB65 set of various dispersion-bound and hydrogen-bonded dimers[65] and other systems containing vdW interactions[39,66]. Since this is a GGA functional, it is susceptible to delocalization error. Other possible approaches are to pair full exact exchange with PBE correlation or to use a hybrid functional that includes a certain fraction of exact exchange.

C. HF exchange and hybrid functionals

In Hartree-Fock (HF) theory, the energy is calculated self-consistently for a Slater determinant wavefunction composed of single-particle HF orbitals[21]. The HF energy includes the kinetic energy of single-particle HF orbitals, nuclear-electron attraction energies, the self-repulsion energies, and the exchange energy. HF is an exact treatment for exchange, however, HF treats the movement of electrons in a mean-field approximation, which does not treat electron correlation[21,67]. Mathematically, the HF exchange energy is expressed as a sum over occupied HF orbitals, and integrated with respect to two distinct electronic coordinates $\boldsymbol{r}_1$ and $\boldsymbol{r}_2$, which is a feature of a non-local functional

$$E_{X\sigma} = -\frac{1}{2}\sum_{ij}\int\int \frac{\psi_{i\sigma}(\boldsymbol{r}_1)\psi_{j\sigma}(\boldsymbol{r}_1)\psi_{i\sigma}(\boldsymbol{r}_2)\psi_{j\sigma}(\boldsymbol{r}_2)}{r_{12}} d^3\boldsymbol{r}_1 d^3\boldsymbol{r}_2. \tag{41}$$

The inclusion of HF exchange in density functionals is popular because it accounts for non-local effects and it is not prone to delocalization error. The exchange-correlation energy including full HF exchange from Eq. 41, PBE correlation, and XDM is

$$E_{xc}^{\mathrm{HFPBE}} = E_x^{\mathrm{HF}} + E_c^{\mathrm{PBE}} + E_{disp}^{\mathrm{XDM}}. \tag{42}$$

However, using HF exchange increases the computational cost and PBE correlation is semilocal, which is not fully compatible with non-local exchange. The pairing of non-local exchange with a semilocal functional is terrible for thermochemistry[68]. An improved possibility is to use a hybrid functional that includes a mixture of both HF and PW86 exchange, paired with PBE correlation and XDM, which is

$$E_{xc}^{\mathrm{PW1PBE}} = cE_x^{\mathrm{HF}} + (1-c)E_x^{\mathrm{PW86}} + E_c^{\mathrm{PBE}} + E_{disp}^{\mathrm{XDM}} \tag{43}$$

where c is the fraction of HF exchange, the value of which is determined from fitting to a training set of atomization energies such as the 222 compounds in the G3/99 set[69]. This approach was originally and popularly applied to construct hybrid functionals such as the Becke-3-Parameter-Lee-Yang-Parr (B3LYP) hybrid[68]. The B97-D functional[29], which adds a dispersion-correction term to Becke-97 functional[30], is also a hybrid GGA that uses a small fraction of exact exchange, but it was fitted with 10 parameters. Results for the PW86PBE-XDM, HFPBE-XDM, and PW86PBE-XDM hybrid (which we denote PW1PBE-XDM) functionals as well as the B97-D functional will be benchmarked against reference CCSD(T) data for vdW PES in the following sections.

D. Computational details

All calculations in this work were performed using the GAUSSIAN 09 program[70] and POSTG[39,65], an external program to run XDM computations. Jacobi coordinates were used to construct the PES for all Rg-linear dimers. The geometries of the linear molecules were optimized for each functional as a systematic approach to determine fixed bond lengths (denoted as r_{eq}), while reference CCSD(T) computations taken from literature sources used experimental bond lengths. The BEs were computed as the magnitude of the energy difference between the vdW molecule, E_{RgX}, and the

sum of monomer energies (the Rg atom, E_{Rg} and the linear molecule, E_X) for each bond length R and bond angle θ

$$\mathrm{BE} = |E_{RgX}(r_{eq}, R, \theta) - E_{Rg} - E_X|. \tag{44}$$

The linear molecule was treated as a rigid rotor, where motions of the nuclei were frozen and intermolecular vibrations were neglected. The calculation of the PES with XDM-corrected functionals was done in two steps. First, self-consistent-field (SCF) energies from the base functionals were computed with GAUSSIAN 09, then the POSTG program was used to calculate XDM dispersion energies from the resulting wavefunction (GAUSSAN 09 .wfx files). For B97-D, the PES calculations were performed directly with GAUSSIAN 09. For geometry optimizations of the vdW molecule, the coordinates of the linear molecule were held fixed and only the coordinates of the Rg atom were allowed to optimize. Geometry optimizations for base functional-XDM were carried simultaneously using both programs, while B97-D calculations were performed directly with GAUSSIAN 09 alone.

Since the PES are relatively flat for Rg-linear complexes, a large integration grid is necessary. The integration grid in DFT calculations uses the Lebedev quadrature scheme. Meta-GGA functionals are sensitive to integration grids[71,72]. Calculations of the potential energy curves of Rg dimers with default integration grids showed spurious oscillations due to numerical noise[72]. Preliminary calculations of the PE curves of the Rg dimers with HFPBE-XDM and PW86PBE-XDM with the Lebedev quadrature scheme of 200 radial grid points and 590 angular grid points showed that numerical noise was present around the minimum. But with a larger quadrature scheme of 200 radial grid points and 974 angular grid points, the PE curves were smooth and free from numerical noise. Thus, we used the (200,974) quadrature scheme for all of the calculations.

The damping function from Eq. 20 is necessary to make the base functionals compatible with XDM. The damping parameters were obtained from minimizing

the root-mean-square (RMS) percent error in calculated BEs related to reference data for a given training set. Optimized damping parameters for PW86PBE-XDM were obtained for the KB65 set[65] that includes hydrogen-bonding, dispersion, electrostatic, and stacking interactions along with Rg dimers. The damping parameters for PW86PBE-XDM from the KB65 set are $a_1 = 0.7564$ and $a_2 = 1.4545$ Å with the Woon and Dunning augmented correlation-consisted triple-zeta (aug-cc-pVTZ) basis set[73] (aug-cc-pV5Z for Rg atoms). The damping parameters for HFPBE-XDM are $a_1 = 0.5955$ and $a_2 = 1.5076$ Å with the aug-cc-pV5Z basis set, determined by fitting only to the set of 10 Rg dimers due to the poor performance of the HFPBE functional for hydrogen-bonding systems. For PW1PBE-XDM, the fraction of HF exchange is $c = 0.1732$, which was obtained by fitting to the atomization energies from the G3/99 set[69]. The damping parameters are $a_1 = 0.8834$ and $a_2 = 1.0715$ Å which are obtained by minimizing the RMS error for the KB65 set. Larger basis sets than aug-cc-pVTZ are still compatible with the damping parameters.

We selected a large aug-cc-pV5Z for Rg atoms since these atoms are sensitive to basis-set superposition error (BSSE). For Rg-diatomic dimers, we use the aug-cc-pV5Z basis set for all atoms although we used a mixed basis set for larger Rg-linear dimers with aug-cc-pVQZ for the triatomic and tetraatomic linear molecules since this is more computationally more affordable. In addition, we decided not to perform counterpoise corrections since DFT methods are less susceptible to BSSE than wavefunction methods like CCSD(T) and XDM is not parameterized to work with CP corrections in order to treat intermolecular and intramolecular interactions on equal footing.

The vdW molecules mentioned in Sec.I were selected based on the availability of CCSD(T) reference data. The majority of the PES in the roster of vdW molecules are based on a rigid rotor model. For some of the vdW molecules (Kr-N_2[74], Ne-CO[75], Ar-CO[76], He-CO_2[77], Ne-CO_2[78], and Kr-CO_2[79]), only vibrationally averaged PES are available in the literature. In general, rigid-rotor PES are preferred for this benchmark study since they are directly comparable to the DFT results. However, the

differences between the rigid-rotor and vibrationally averaged PES are quite small. The vibrationally averaged values for Ar-OCS[80] (R = 3.650 Å, θ = 106.10°, BE = 227.28 cm^{-1}) and Kr-OCS[81] (R = 3.783 Å, θ = 103.50°, BE = 271.23 cm^{-1}) are comparable with the rigid-rotor values listed on Tables I-III. Therefore, we included vdW molecules with vibrationally averaged PES in this benchmark study.

For consistency, we choose a combination of points that matches the boundaries, dimensions, and units of the CCSD(T) PES, as summarized in Appendix A in Table A.2. For most of the PES, the contours are expressed in wavenumbers (cm^{-1}) and some PES may use milihartrees (mE_h). Additional energy points may be included to plot smoother contours for the PES. The contours of the PES are visualized with MATLAB[82] for qualitative comparisons with the reference PES. We will not fit our PES analytically since we will not perform any spectroscopic calculations. We note that authors who performed CCSD(T) calculations for Kr-HF obtained accurate results, but they accidentally flipped the description of their Jacobi coordinates. We performed a test calculation for Kr-HF with CCSD(T), which verified that the minimum-energy arrangement corresponds to the Kr-H-F geometry, which should occur for a bond angle of 0°.

III. RESULTS AND DISCUSSION

A. Comparison of PES

We assess the quality of the PES of base-XDM functionals and B97-D by comparing both the minimum BEs for the global minima and anisotropies of the CCSD(T) PES. In this section, we focus on the appearance of the computed PES. A satisfactory PES must reproduce the correct anisotropy of the vdW interaction, which means that the PES contains the correct number of minima, corresponding to the same geometries, and with values of the BEs in agreement with the CCSD(T) reference data. In this section, we identify cases where base-XDM and B97-D functionals describe the anisotropies and BEs within acceptable accuracy. In addition, we explore problematic cases where dispersion-corrected functionals obtain incorrect geometries at the minimum with adequate accuracy of the BEs, cases with incorrect BEs only, and cases where BEs and geometries at the minimum are incorrect. Performance of individual functionals is discussed based on overall trends and deviations observed from the calculations. As discussed previously, base functionals without XDM fail to predict the correct anisotropy and global minimum BEs of vdW molecules, normally predicting very weak binding interactions or unbound complexes. We select noteworthy examples of PES of certain vdW molecules to guide the assessment of the functionals and the remaining PES plots for all dispersion-corrected functionals are shown in Appendix B.

The XDM-corrected functionals and B97-D perform relatively well, reproducing the correct shape and anisotropy of the PES for Rg-N_2, Rg-H_2, Rg-CO_2, Rg-CO, and Rg-OCS complexes and obtaining satisfactory global minimum BEs in comparison with CCSD(T). For Rg-N_2 and Rg-CO_2, the most preferable geometry (i.e. the global minimum) is T-shaped[74,77–79,83,85] as shown in Fig. 2 for Ar-N_2 as a representative example (the contour lines represent energy level relative to the infinitely separated monomers). In addition, the functionals predict the following correct geometries

FIG. 2. PES of Ar-N_2 with XDM-corrected functionals and B97-D.

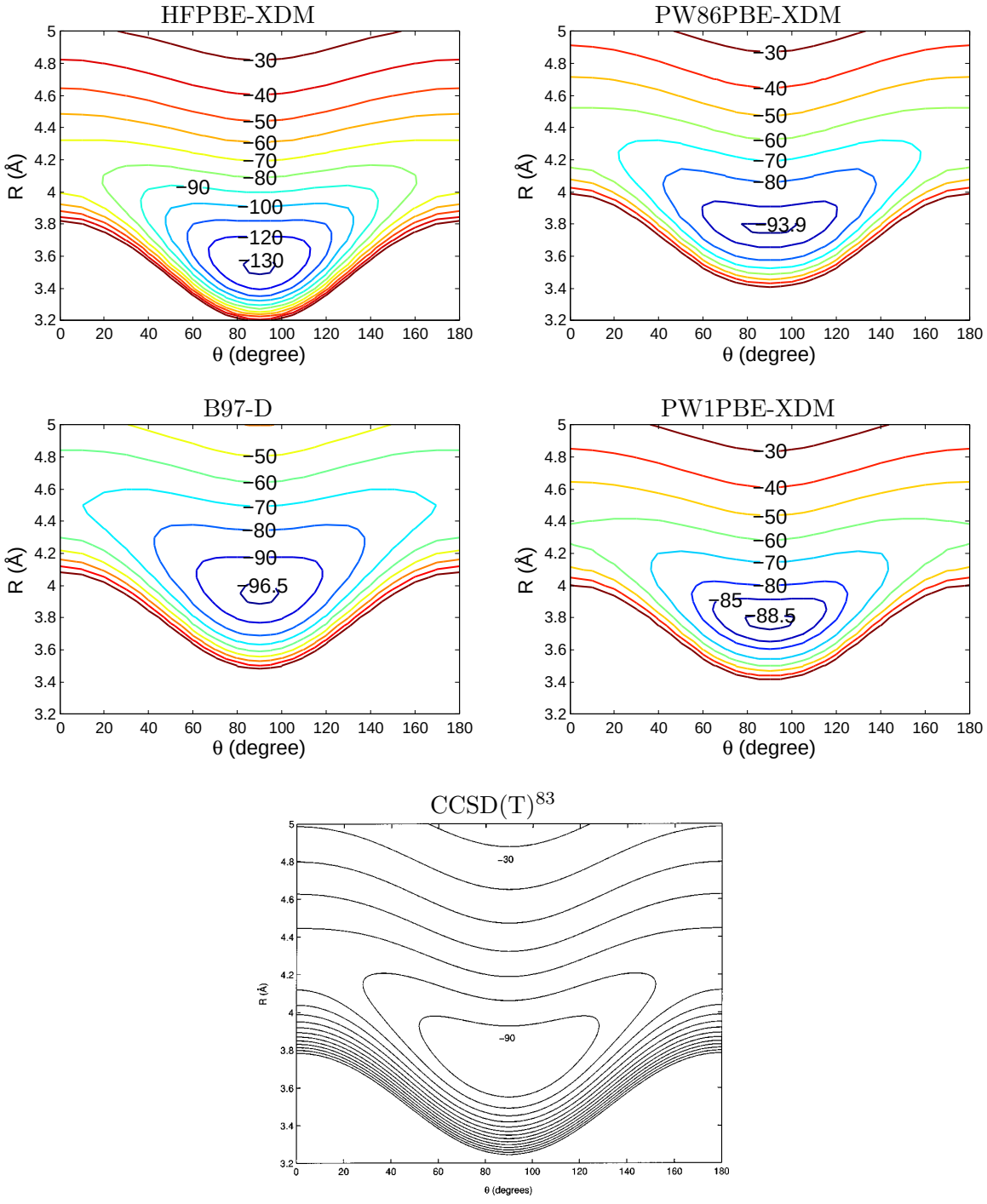

FIG. 3. PES of Ar-C_2H_2 with XDM-corrected functionals and B97-D.

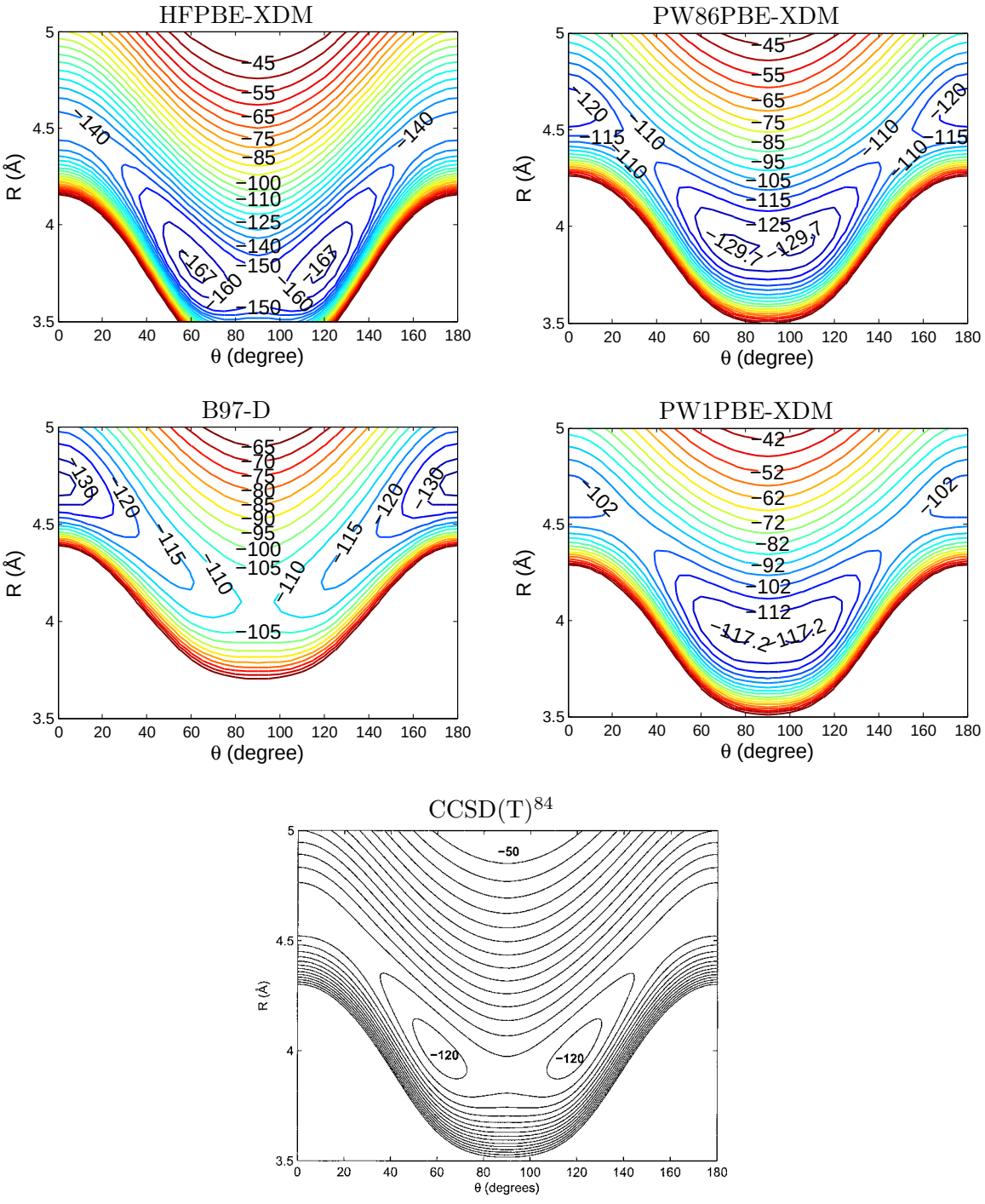

for the remaining compounds in this set: the secondary minima at the collinear arrangement for He-CO_2[77], Ne-CO_2[78], and Rg-OCS[86–88], a collinear geometry at the global minimum for Rg-H_2[89,90], and distorted T-shaped geometries for Rg-CO[75,76,91,92] and Rg-OCS[86–88]. However, PW86PBE-XDM predicts a distorted T-shaped geometry instead of a perfect T-shape arrangement[74] for Kr-N_2. With the inclusion of exact exchange with the hybrid functional, PW1PBE-XDM, the global minimum geometry is restored to the correct T-shape. In general, all dispersion-corrected functionals obtain appropriate geometries and satisfactory BEs for this set of Rg-linear vdW molecules. This shows that the functionals are able to treat dispersion interactions for Rg-linear nonpolar and Rg-linear moderately polar dimers, since the dispersion interaction is the main contribution to the stability of these complexes. As previously mentioned in Sec.II D, several vdW molecules only have vibrationally averaged PES available for this sensitive test. The inclusion of these PES are appropriate since the vibrationally averaged PES retains the same shape as the PES of vdW molecules that are treated as a rigid rotor, as exemplified from the PES of Ar-OCS[80,87] and Kr-OCS[81,88], respectively. Fortunately, the shapes of the PES of these vdW molecules from DFT methods agrees quite well with vibrationally averaged PES.

The Rg-C_2H_2 dimers are problematic cases for predicting correct anisotropies with all functionals due to the flatness of the PES[93], as shown for the example of Ar-C_2H_2 in Figure 3. For instance, B97-D predicts a favorable pseudo-hydrogen-bonding interaction between the noble gas atoms (Ne, Ar, and Kr) and the H atom from the C_2H_2 molecule at the collinear geometry while the global minima for these complexes are distorted T-shaped geometries[84,94]. Both PW86PBE-XDM and PW1PBE-XDM predict incorrect anisotropies as follows: a distorted T-shape secondary minimum for He-C_2H_2; a perfect T-shape global minimum for Ne-C_2H_2; and less-distorted T-shape global minima for Ar-C_2H_2 and Kr-C_2H_2, which are nearly perpendicular to the axis of the C_2H_2 molecule. It is possible that PW86PBE and B97-D have difficulties in treating interactions involving the π system of the C-C bond in C_2H_2. Moreover, the addition of a small portion of exact exchange along with XDM for the hybrid

functional does not fix the incorrect anisotropy of the Rg-C_2H_2 interaction, unlike the Kr-N_2 case. Only HFPBE-XDM predicts the correct anisotropies for Ne-C_2H_2, Ar-C_2H_2, and Kr-C_2H_2 where the shapes are equivalent to the CCSD(T) PES plots. Because the PES of Rg-C_2H_2 are so flat around the π region of C_2H_2, the results are susceptible to small errors in the repulsive exchange-only curves from the base functional. However, full exact exchange is capable of providing a qualitatively correct picture of these PES when paired with XDM.

The Rg-HCN complexes also reveal difficulties in predicting the correct anisotropies with the dispersion-corrected functionals. All PES of Rg-HCN dimers have a global minimum at the Rg-HCN arrangement[95] where hydrogen bonding is favored due to the high polarity of the HCN molecule. Most of the functionals obtain the correct global minimum. The number of local minima for Rg-HCN complexes, which are present at the T-shaped configurations between 50° to 60°. and 100° to 110°, differ depending on the Rg atom. For He-HCN, there is only one local minimum at the T-shaped configuration, Ne-HCN has two local minima at the T-shaped arrangement and the third local minimum is at the Ne-NCH collinear geometry, and both Ar-HCN and Kr-HCN have two T-shaped local minima[95]. The anisotropy problems for Rg-HCN PES with the dispersion-corrected functionals bear some slight similarities with the problematic cases of Rg-C_2H_2, but with some differences. HFPBE-XDM predicts a global minimum at a distorted T-shaped geometry tilting towards the H atom for Ar-HCN and Kr-HCN rather than the collinear arrangement where the Rg atom aligns with the H atom of HCN, although it predicts the linear arrangement for He-HCN and Ne-HCN. The polarizability of Ar and Kr might influence the global minimum for HFPBE-XDM, which favors dispersion interactions with the π region. In terms of anisotropies of the PES of Rg-HCN complexes, the functionals do not identify all other local minima since the PES around the local minima predicted by CCSD(T) are quite flat and these functionals are apparently not sensitive enough to capture those interactions.

The Rg-hydrogen halide dimers are relatively stable due to both induction and dispersion interactions, owing to the permanent dipole moments of the hydrogen halide molecules. Two minima are present: the first where the Rg atom aligns nearest the H atom (pseudo-hydrogen-bonding) and the second structure where the Rg atom aligns nearest the halogen (F, Cl, and Br), where dispersion dominates due to the polarizability of the heavier halogens. Here, we cover Rg-HCl and Rg-HBr complexes separately from Rg-HF since the latter involve different issues with respect to the performance of the functionals.

The Rg-HCl and Rg-HBr dimers reveal problems predicting correct anisotropies with dispersion-corrected functionals, similar to the Rg-C_2H_2 and Rg-HCN complexes. Since HCl and HBr are moderately polar molecules, the Rg-H-X and Rg-X-H (X = Cl, Br) collinear minima are competing structures where the differences in the BEs between those configurations are small. For He-HCl, all functionals favor pseudo-hydrogen-bonding between the He atom and the H atom, which is the opposite to what is observed in the CCSD(T) PES of He-HCl[97] although the two minima are very nearly degenerate. However for Ne-HCl and Ne-HBr, the behavior is reversed and CCSD(T) favors the global minimum configuration as the pseudo-hydrogen-bonding interaction between Ne and the H-atom[98,99]. HFPBE-XDM is the only functional that incorrectly predicts the global minimum at the Ne-X-H configuration, favoring dispersion between the heavy halogen atom and Ne. The flatness of these PES is a concern for HFPBE-XDM, which obtains global minimum geometries that contrast with CCSD(T) reference data. However, HFPBE-XDM performs better in terms of the shapes and the curvature of the PES, and their minima are quite close in energy. We note that the defined Jacobi coordinates for Ne-HBr[99] are slightly different since the Ne atom aligns to the Br atom rather than the center of mass of HBr. The results are not affected since the center of mass is extremely close to the Br atom.

The Rg-HF dimer is a particularly problematic case for XDM-corrected functionals and B97-D. Since HF is quite polar, the preferred global minimum is the pseudo-hydrogen-bonding interaction between the Rg atom and H at the collinear

FIG. 4. PES of Kr-HF with XDM-corrected functionals and B97-D. The bond length is aligned at the horizontal axis of the reference PES.

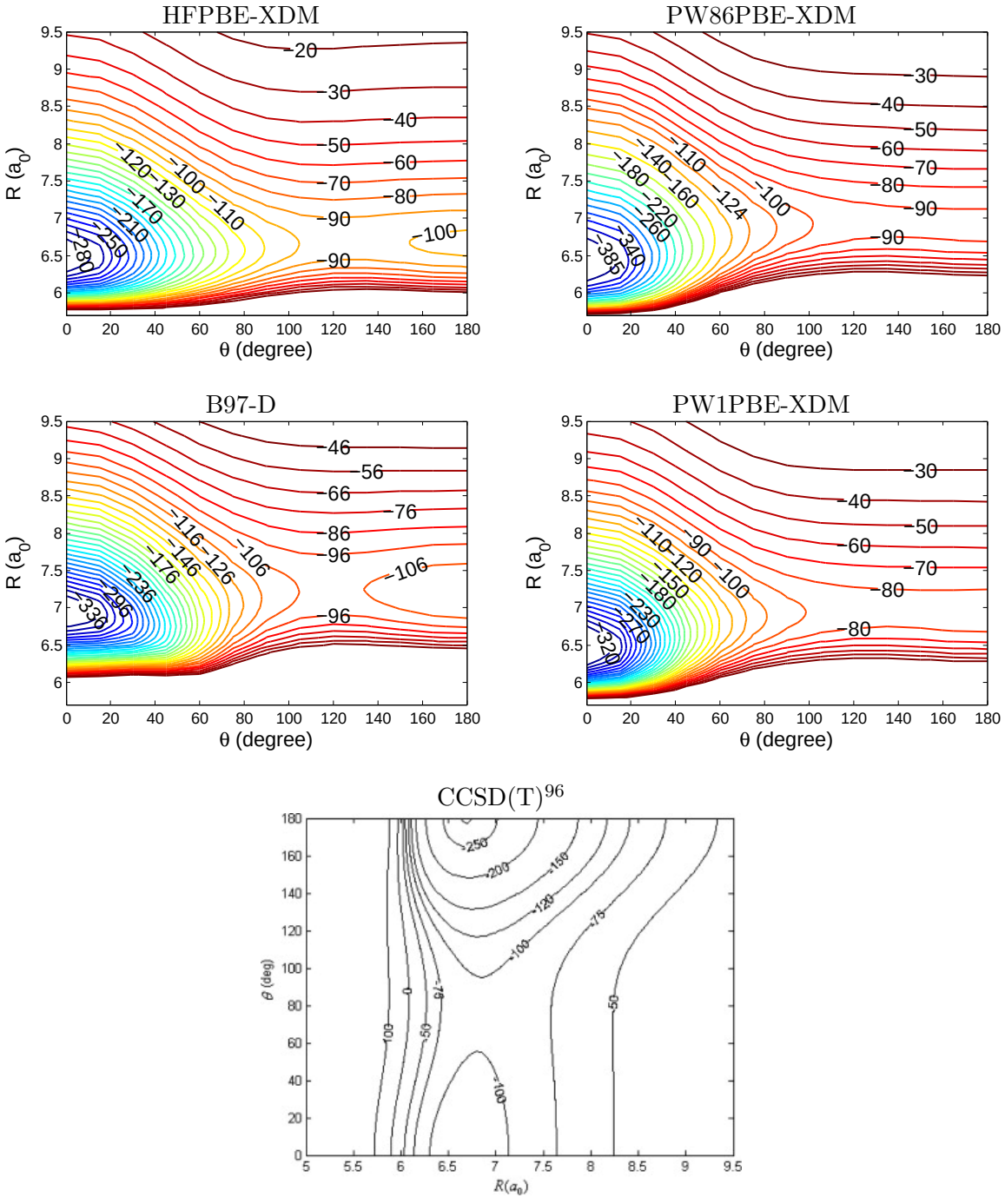

FIG. 5. PES of Kr-HF with selected base functionals.

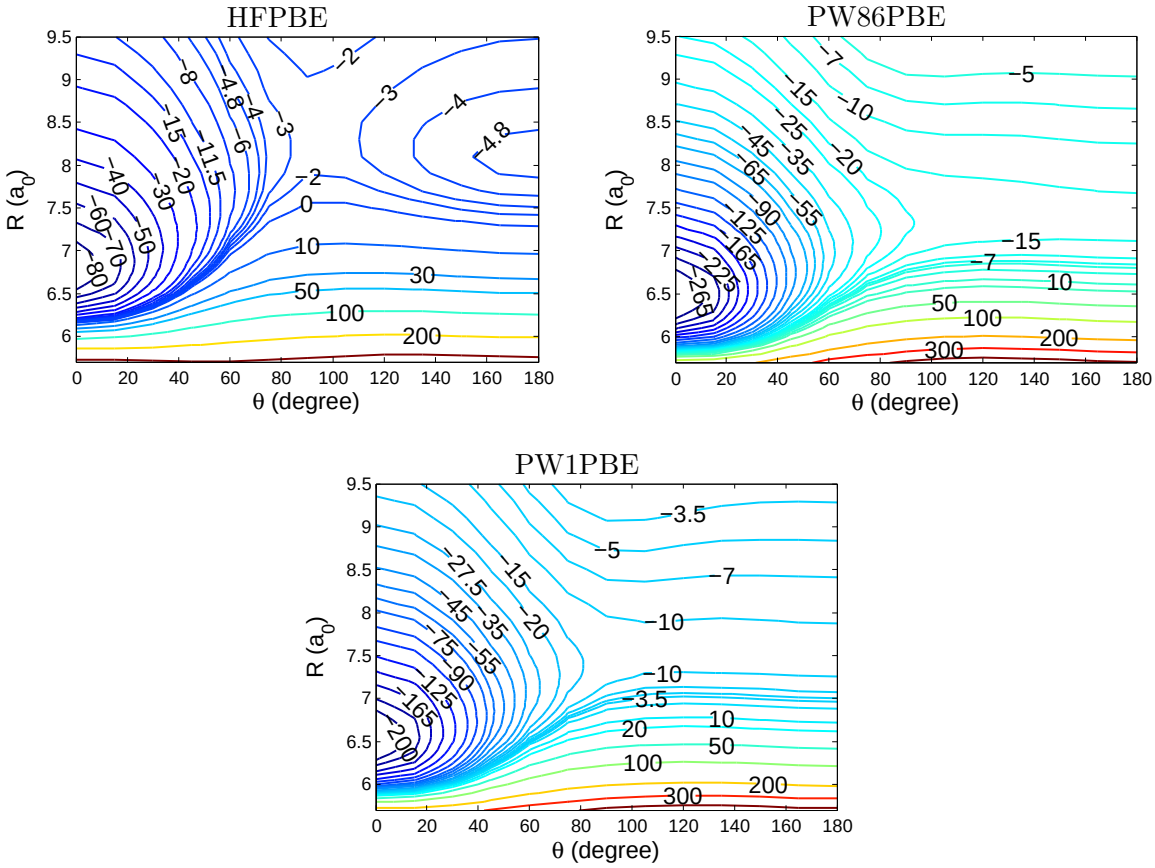

geometry[96,100]. Before proceeding to our discussion, the Jacobi coordinates of the global minimum for Kr-HF are noteworthy since the authors of the CCSD(T) study claimed that the global minimum is at the Kr-F-H arrangement[96]. The work on Xe-HF[101] follows a similar trend while studies of He-HF[100] and Ne-HF[102] do not. We claim that the authors who performed the calculations on Kr-HF and Xe-HF accidentally flipped the definition of the angular coordinates, which was verified by our test calculations using CCSD(T); the global minimum is actually the pseudo-hydrogen-bonding interaction.

From the PES plots of Kr-HF in Fig. 4, PW86PBE-XDM severely overbinds the Kr-HF interaction as indicated from the PES and the secondary Kr-F-H local minimum is not even present. The He-HF complex follows the same trend as Kr-HF, but

to a much lesser extent. The addition of exact exchange to PW86PBE-XDM slightly improves the BEs for He-HF and Kr-HF, but it does not fix the incorrect shape of the PES at the secondary minimum. From Fig. 5 for Kr-HF, PW86PBE and the hybrid predict a strong binding interaction between Kr and HF even without XDM. This overly-strong bonding between the Rg atom and HF suggests that PW86PBE suffers from delocalization error due to a nonphysical charge transfer between the Rg atom and HF, where the Rg atom becomes charged. The charge on Kr for the minimum with PW86PBE-XDM is 0.038. This fractional charge transfer leads to artificially large binding, and this phenomenon is well known to occur as a result of delocalization error. For Rg-HF, HFPBE-XDM, which does not suffer from delocalization error, performs the best and it reproduces BEs and anisotropies comparable to CCSD(T).

B. Binding energies

We optimized the molecular geometries of all Rg-linear vdW molecules at the global minima with XDM-corrected functionals and B97-D and computed the BEs using Eq. 44. Based on mean absolute errors (MAE) for the BEs in Table I, bond angles in Table II, and bond lengths in Table III, the PW1PBE-XDM hybrid performs the best compared to other dispersion-corrected functionals. This indicates that addition of exact exchange improves PW86PBE-XDM for most of the vdW molecules.

In general, HFPBE-XDM predicts shorter bond lengths than CCSD(T) while B97-D and PW86PBE-XDM predict longer bond lengths, and PW1PBE obtains bond lengths closest to CCSD(T), with the exception of the Rg-HF complexes. Some of the bond lengths may differ significantly when the position of the global minimum is different from CCSD(T). In terms of bond angles, all dispersion-corrected functionals predict relatively good agreement in the bond angles for most of the vdW molecules, although there are cases again where the functionals obtain a global minimum BE at a different geometry. Examples include the collinear hydrogen bonding interaction

of Ne-C_2H_2, Ar-C_2H_2, and Kr-C_2H_2 by B97-D, the distorted T-shaped minimum for Ar-HCN and Kr-HCN rather than hydrogen bonding by HFPBE-XDM, and the distorted T-shaped minimum predicted by PW86PBE-XDM for Kr-N_2. There are instances where the inclusion of HF exchange with PW86PBE-XDM restores the agreement with reference geometries, such as Kr-N_2, but not Rg-C_2H_2 where the anisotropy computed by PW86PBE-XDM remains.

TABLE I: Global minimum BEs of the Rg-linear vdW molecules with XDM-corrected functionals, B97-D, and CCSD(T) in cm^{-1}.

Rg	**Molecule**	**HFPBE**	**PW86PBE**	**PW1PBE**	**B97-D**	**CCSD(T)**
Ne	H_2	25.44	32.97	28.24	48.27	21.46[89]
Kr	H_2	90.27	81.92	69.63	78.65	61.76[90]
Ne	N_2	57.87	50.86	48.99	74.44	49.50[85]
Ar	N_2	131.30	94.15	89.17	97.26	99.01[83]
Kr	N_2	164.47	112.27	105.22	127.50	112.01[74]
He	CO	28.48	22.77	22.59	32.56	22.02[91]
Ne	CO	61.68	53.78	50.75	70.95	49.41[75]
Ar	CO	148.12	108.29	97.97	93.84	102.00[76]
Kr	CO	190.77	136.06	120.80	125.28	119.68[92]
He	HF	45.46	67.00	56.30	82.04	43.84[100]
Kr	HF	291.97	415.70	341.61	350.32	252.35[96]
He	HCl	32.10	35.72	30.41	49.85	32.74[97]
Ne	HCl	63.51	85.02	68.33	114.67	66.85[98]
Ne	HBr	76.99	77.34	62.35	109.64	58.60[99]
He	CO_2	60.12	40.90	40.92	53.10	49.39[77]
Ne	CO_2	107.20	77.01	75.06	113.40	93.05[78]
Kr	CO_2	325.71	207.40	192.06	221.17	231.70[79]

TABLE I – Continued

Rg	Molecule	HFPBE	PW86PBE	PW1PBE	B97-D	CCSD(T)
Ne	OCS	109.12	82.68	78.81	112.20	81.26[86]
Ar	OCS	291.96	186.52	173.46	162.91	221.05[87]
Kr	OCS	387.30	234.44	217.71	226.61	270.73[88]
He	HCN	33.76	31.90	28.08	51.55	29.90[95]
Ne	HCN	66.48	72.94	62.06	115.73	56.97[95]
Ar	HCN	184.55	165.94	145.09	177.03	147.00[95]
Kr	HCN	246.83	211.72	184.57	243.41	179.00[95]
He	C_2H_2	27.33	25.62	21.90	43.35	24.22[84]
Ne	C_2H_2	56.63	60.42	52.90	96.56	50.20[84]
Ar	C_2H_2	168.83	130.41	117.59	134.40	122.17[84]
Kr	C_2H_2	234.43	165.73	150.69	185.96	151.88[94]
MAE		32.75	18.44	12.33	29.94	
MAPE		27.71	17.66	10.27	43.22	

TABLE II: Bond angles corresponding to the global minima of Rg-linear vdW molecules with XDM-corrected functionals, B97-D, and CCSD(T) in degrees.

Rg	Molecule	HFPBE	PW86PBE	PW1PBE	B97-D	CCSD(T)
Ne	H_2	0.00	0.00	0.00	0.00	0.00[89]
Kr	H_2	0.00	0.00	0.00	0.00	0.00[90]
Ne	N_2	90.00	90.00	90.00	90.00	90.00[85]
Ar	N_2	89.83	89.79	90.00	90.00	90.00[83]
Kr	N_2	90.04	106.81	90.00	90.00	90.00[74]
He	CO	87.05	80.68	80.82	82.50	70.81[91]
Ne	CO	89.31	95.43	89.06	86.75	82.50[75]

TABLE II – Continued

Rg	Molecule	HFPBE	PW86PBE	PW1PBE	B97-D	CCSD(T)
Ar	CO	95.43	104.21	99.42	92.10	93.00[76]
Kr	CO	97.94	108.33	103.87	97.55	98.50[92]
He	HF	0.00	0.00	0.00	0.00	0.00[100]
Kr	HF	0.00	0.00	0.00	0.00	0.00[96]
He	HCl	0.00	0.00	0.00	0.00	180.00[97]
Ne	HCl	180.00	0.00	0.00	0.00	0.00[98]
Ne	HBr	180.00	0.00	0.00	0.00	0.00[99]
He	CO_2	90.00	90.00	90.00	90.00	90.00[77]
Ne	CO_2	90.00	90.00	90.00	90.00	90.00[78]
Kr	CO_2	90.00	90.00	90.00	90.00	90.00[79]
Ne	OCS	108.13	105.25	106.69	106.80	108.46[86]
Ar	OCS	104.79	103.65	104.41	105.00	105.98[87]
Kr	OCS	103.75	102.78	103.34	100.56	105.00[88]
He	HCN	0.00	0.00	0.00	0.00	0.00[95]
Ne	HCN	0.00	0.00	0.00	0.00	0.00[95]
Ar	HCN	63.70	0.00	0.00	0.00	0.00[95]
Kr	HCN	65.93	0.00	0.00	0.00	0.00[95]
He	C_2H_2	0.00	0.00	0.00	0.00	0.00[84]
Ne	C_2H_2	47.94	90.00	90.00	0.00	43.30[84]
Ar	C_2H_2	61.25	75.08	75.24	0.00	60.60[84]
Kr	C_2H_2	66.55	74.01	75.16	0.00	65.22[94]
MAE		25.19	11.38	10.17	13.36	

TABLE III: Bond lengths corresponding to the global minima of the Rg-linear vdW molecules with XDM-corrected functionals, B97-D, and CCSD(T) in Å.

Rg	Molecule	HFPBE	PW86PBE	PW1PBE	B97-D	CCSD(T)
Ne	H_2	3.307	3.254	3.295	3.387	3.312[89]
Kr	H_2	3.565	3.664	3.708	3.800	3.761[90]
Ne	N_2	3.278	3.415	3.401	3.530	3.380[85]
Ar	N_2	3.534	3.769	3.770	3.950	3.709[83]
Kr	N_2	3.649	3.938	3.916	4.029	3.862[74]
He	CO	3.241	3.406	3.386	3.571	3.399[91]
Ne	CO	3.250	3.419	3.395	3.535	3.386[75]
Ar	CO	3.506	3.787	3.776	3.955	3.720[76]
Kr	CO	3.620	3.929	3.923	4.023	3.888[92]
He	HF	3.047	2.966	2.994	3.124	3.166[100]
Kr	HF	3.428	3.390	3.420	3.670	3.544[96]
He	HCl	3.758	3.715	3.761	3.863	3.349[97]
Ne	HCl	3.388	3.697	3.750	3.800	3.833[98]
Ne	HBr	3.430	3.962	4.021	4.050	4.070[99]
He	CO_2	2.926	3.124	3.098	3.331	3.063[77]
Ne	CO_2	3.032	3.224	3.211	3.336	3.153[78]
Kr	CO_2	3.392	3.649	3.651	3.741	3.571[79]
Ne	OCS	3.292	3.453	3.458	3.605	3.474[86]
Ar	OCS	3.470	3.737	3.744	3.941	3.669[87]
Kr	OCS	3.562	3.856	3.863	3.947	3.780[88]
He	HCN	4.091	4.128	4.135	4.212	4.216[95]
Ne	HCN	4.124	4.120	4.149	4.181	4.248[95]
Ar	HCN	3.633	4.398	4.418	4.505	4.497[95]

TABLE III – Continued

Rg	Molecule	HFPBE	PW86PBE	PW1PBE	B97-D	CCSD(T)
Kr	HCN	3.703	4.519	4.540	4.591	4.634[95]
He	C_2H_2	4.289	4.313	4.338	4.400	4.350[84]
Ne	C_2H_2	3.789	3.597	3.623	4.345	3.950[84]
Ar	C_2H_2	3.773	3.904	3.918	4.708	3.990[84]
Kr	C_2H_2	3.795	4.013	4.026	4.770	4.064[94]
MAE		0.249	0.099	0.082	0.189	

Based on the MAE results for the BEs in Table I for the entire set of vdW complexes, HFPBE-XDM and B97-D perform worse compared to the other functionals. HFPBE-XDM and B97-D tend to overestimate the BEs, while PW86PBE-XDM and the hybrid provide lower MAEs. However, using the MAE alone is not the most effective approach to gauge the performance of these functionals since the BEs span such a large range. The mean-absolute-percent error (MAPE) is more appropriate to describe the trends in the BE errors for each functional. We also assess the error trends with respect to the size of the Rg atom and with respect to the polarity of the linear molecule in Table IV. In our set of vdW molecules, there are six molecules that pair with He, nine with Ne, five with Ar, and eight with Kr. In our set of linear molecules, there are four nonpolar molecules (H_2, N_2, CO_2 and C_2H_2), four polar molecules with moderate polarity (CO, OCS, HBr, and HCl), and two very polar molecules with large dipole moments (HF and HCN). We tabulate the MAPEs of the vdW molecules and group the errors with respect to the size of the Rg atom and the polarity of the linear molecules for all functionals in Table IV. We note that we do not have the complete set for other Rg-linear vdW molecules due to the lack of accurate CCSD(T) reference data in the literature.

Based on the MAPEs for the entire set of Rg-linear vdW molecules, the PW86PBE-XDM hybrid performs the best while B97-D performs the worst. This suggests, at

TABLE IV. Mean Absolute Percent Error (MAPE) of the BEs for base-XDM functionals and B97-D with respect to the size of the Rg atom and the polarities of the linear molecule.

Roster	**HFPBE**	**PW86PBE**	**PW1PBE**	**B97-D**
Full	27.71	17.66	10.27	43.22
He	13.74	15.82	11.82	57.76
Ne	19.52	21.19	8.95	70.34
Ar	34.73	9.26	8.09	13.30
Kr	43.00	20.32	11.96	20.49
nonpolar	29.73	15.00	11.20	38.03
polar	30.65	13.11	7.00	39.57
highly polar	18.74	30.57	13.87	59.65

first glance, that the PW86PBE-XDM hybrid works nicely while B97-D has difficulties in obtaining the correct BEs. Since B97-D, by construction, is a hybrid GGA parameterized for organic molecules with an empirical correction, it does not model the exchange repulsion well for Rg complexes. Since this functional is built on fitting parameters to minimize the error for a test set, B97-D does not guarantee accuracy and applicability to describe vdW interactions accurately for systems such as these that fall outside the training set. HFPBE-XDM also has trouble computing accurate BEs since the HFPBE functional does not include a balanced treatment of correlation. The PW86PBE-XDM functional seems to perform quite well since it mimics the HF exchange contribution to the PES well for Rg dimers, but the inclusion of exact exchange improves the BEs even further. We will explore these errors in greater detail in terms of the size of the Rg atoms and the polarities of the linear molecules.

Upon inspection of the MAPEs in the BEs for various Rg atoms, the errors for HFPBE-XDM increases with increasing size of the Rg atom. This indicates that the performance of HFPBE-XDM is size-dependent. Since HFPBE-XDM does not treat correlation correctly, the HFPBE functional performs worse for larger Rg atoms where

electron correlation becomes more important. In contrast, B97-D performs worse for vdW molecules containing smaller Rg atoms, since it is empirical and these systems fall outside the training set, while it performs decently for larger Rg atoms. The source of error is incorrect behavior of the exchange-repulsion part of PES involving vdW molecules with small Rg atoms. The PW86PBE-XDM functional performs adequately with respect to reference CCSD(T) data, but the errors are larger for complexes involving Ne. The BE errors for PW1PBE-XDM are consistently lower than PW86PBE-XDM and HFPBE-XDM, which indicates that the hybrid functional compensates the errors in the GGA by including some exact exchange, while retaining a large fraction of PW86 exchange to pair well with PBE correlation. For PW86PBE-XDM and PW1PBE-XDM, the BE errors are not proportional to the size of the Rg atom.

As seen from the MAPEs in the BEs for varying polarity, GGA functionals tend to perform worse for highly polar linear molecules. B97-D, in particular, mostly underperforms, giving the highest MAPE for vdW molecules involving HF and HCN. This suggests that B97-D overbinds these complexes significantly due to delocalization error. The performance of HFPBE-XDM is decent, but it still gives larger errors for vdW molecules containing nonpolar and moderately polar linear molecules. The source of error in HFPBE is evidently due to difficulties in treating correlation properly. For highly polar molecules, HFPBE-XDM performs comparatively well since it does not suffer from delocalization error, unlike functionals with GGA exchange. The BE errors with HFPBE-XDM are not polarity-dependent, but these arise due to its difficulty in treating correlation for larger Rg atoms. In contrast, PW86PBE-XDM performs quite well for vdW molecules containing nonpolar and moderately-polar molecules. However, the performance of PW86PBE-XDM is concerning for Rg-HF vdW molecules, which contributes to a large MAPE. PW86PBE suffers from delocalization error where charge-transfer overstabilizes the pseudo-hydrogen-bond between the Rg atom and the H atom from HF. The errors of PW86PBE-XDM are not dependent on the size of the Rg atom, but vary depending on the polarity of the linear

molecule and the ability of the complex to experience spurious charge transfer. On the other hand, the PW86PBE-XDM hybrid performs better than all of the other functionals with respect to the polarity of the linear molecule. The errors in the BEs with the PW86PBE-XDM hybrid do not increase with increasing polarity. However, the hybrid does not obtain the correct BEs for Kr-HF and He-HF dimers since delocalization error is still present, although to a lesser extent than with the GGAs.

TABLE V: General performance of functionals.

Functional	**Comments**
B97-D	Pros: Good BEs for vdW molecules with large Rg atoms. Cons: Overbinds vdW molecules with small Rg atoms and polar and highly polar molecules. Incorrect global minimum geometries for Ne-C_2H_2, Ar-C_2H_2, Kr-C_2H_2, and Rg-HCN. Long bond lengths.
HFPBE-XDM	Pros: Does not suffer from delocalization error. Relatively reasonable BEs for vdW molecules with small Rg atoms and highly polar molecules. Cons: Large BE errors for vdW molecules with large Rg atoms, BEs are overbound, incorrect global minimum geometries, for Ne-HCl, Ne-HBr, Ar-HCN, and Kr-HCN. Short bond lengths.
PW86PBE-XDM	Pros: Good BEs and geometries for vdW molecules with non-polar and moderately polar linear molecules. Cons: Overbinds Rg-HF and Rg-HCN due to delocalization error and incorrect geometries for Kr-N_2, Ne-C_2H_2, Ar-C_2H_2, and Kr-C_2H_2.
PW1PBE-XDM	Pros: BEs and geometries in agreement with CCSD(T) reference data. Reduces delocalization error relative to PW86PBE-XDM. Cons: Kr-HF is overbound and incorrect geometries for Ar-C_2H_2, Kr-C_2H_2, and Rg-HCN.

IV. SUMMARY AND OUTLOOK

We computed the PES and BEs at optimized geometries for the set of Rg-linear vdW molecules with XDM-corrected functionals and the popular B97-D method. We determined that the PW86PBE-XDM hybrid functional performs better than other functionals for determining BEs, bond lengths, and bond angles. In addition, it reproduces the shapes of the PES from CCSD(T) and it corrects the anisotropies, relative to PW86PBE-XDM, for some of the vdW molecules. In addition, we compare the performance of functionals for problematic vdW molecules: Rg-C_2H_2, Rg-HCN, Ne-HCl, Ne-HBr, and Kr-HF; dimers that are troublesome for GGA functionals. The principal sources of error come from the delocalization error of GGA functionals and the poor treatment of correlation with HFPBE. We highlighted the performance of XDM-corrected functionals and B97-D in terms of the relative size of the Rg atoms and the polarities of the linear molecules. B97-D generally performs poorly for any Rg-linear vdW molecules since it is empirical by design, with a poor treatment of exchange repulsion. HFPBE-XDM performs poorly for larger noble gas atoms. PW86PBE-XDM performs worse for more polar molecules such as HF. Thus, using a fraction of exact exchange and PW86PBE paired with XDM reduces the errors. The quality of the results from the hybrid functional is not size-dependent with respect to the Rg atom and it performs relatively well for vdW molecules with both non-polar and polar monomers. However, this functional does not correct all of the features of the PES since it has a large fraction of PW86 exchange and a large portion of the remaining errors come from the PW86 exchange functional.

We conclude that the PW86PBE-XDM hybrid is the most ideal functional for the considered PES due to its ability to provide consistently accurate results and applicability for the majority of the Rg-linear vdW molecules. HFPBE-XDM and PW86PBE-XDM perform well for certain molecules, but are not as consistent as the hybrid. However, some errors with the hybrid functional are unavoidable due to the remaining delocalization error, even though XDM is an excellent dispersion correc-

tion to pair with this functional. The motivation for applying DFT with dispersion-corrected functionals is promising as long as the effects of delocalization (charge transfer) errors can be reduced. In the future, we may extend our work to benchmark larger closed-shell vdW molecules such as linear-linear and Rg-non-linear complexes to further investigate the performance of the hybrid functional.

REFERENCES

[1]A. J. Stone, *The theory of intermolecular forces*, 2nd ed. (Oxford University Press, Oxford, 2013).

[2]A. D. Buckingham, P. W. Fowler, and J. M. Hutson, Chem. Rev. **88**, 963 (1988).

[3]G. Chałasiński and M. M. Szczęśniak, Chem. Rev. **94**, 1723 (1994).

[4]A. D. Becke, J. Chem. Phys. **138**, 074109 (2013).

[5]J. Klimeš and A. Michaelides, J. Chem. Phys. **137**, 120901 (2012).

[6]J. M. Hutson, Ann. Rev. Phys. Chem. **41**, 123 (1990).

[7]B. L. Blaney and G. E. Ewing, Ann. Rev. Phys. Chem. **27**, 553 (1976).

[8]D. Xie, H. Ran, and Y. Zhou, Int. Rev. Phys. Chem. **26**, 487 (2007).

[9]A. van der Avoird, P. E. S. Wormer, and R. Moszynski, Chem Rev. **94**, 1931 (1994).

[10]S. Boys and F. Bernardi, Mol. Phys. **19**, 553 (1970).

[11]F. Jensen, *Introduction to Computational Chemistry*, 2nd ed. (John Wiley & Sons, 2006).

[12]R. J. Bartlett, Ann. Rev. Phys. Chem. **32**, 359 (1981).

[13]C. Møller and M. S. Plesset, Phys. Rev. **46**, 618 (1934).

[14]K. Raghavachari, G. W. Trucks, J. A. Pople, and M. Head-Gordon, Chem. Phys. Lett. **157**, 479 (1989).

[15]S. M. Cybulski and M. L. Lytle, J. Chem. Phys. **127**, 141102 (2007).

[16]R. J. Bartlett and M. Musiał, Rev. Mod. Phys. **79**, 291 (2007).

[17]B. Jeziorski, R. Moszynski, and K. Szalewicz, Chem. Rev. **94**, 1887 (1994).

[18]K. Szalewicz, Wiley Interdisciplinary Reviews: Computational Molecular Science **2**, 254 (2012).

[19]G. Chałasiński and M. M. Szczęśniak, Chem. Rev. **100**, 4227 (2000).

[20]A. J. Cohen, P. Mori-Sánchez, and W. Yang, Chem. Rev. **112**, 289 (2012).

[21]A. D. Becke, J. Chem. Phys. **140**, 18 (2014).

[22]S. Kristyán and P. Pulay, Chem. Phys. Lett. **229**, 175 (1994).

[23]C. Fiolhais, F. Nogueira, and M. Marques, *A Primer in Density Functional Theory* (Springer-Verlag, New York, 2003).

[24]J. P. Perdew, A. Ruzsinszky, L. A. Constantin, J. Sun, and G. I. Csonka, J. Chem. Theory Comput. **5**, 902 (2009).

[25]J. M. Pérez-Jordá and A. Becke, Chem. Phys. Lett. **233**, 134 (1995).

[26]Y. Zhao, N. E. Schultz, and D. G. Truhlar, J. Chem. Phys. **123**, 161103 (2005).

[27]Y. Zhao and D. G. Truhlar, J. Chem. Phys. **125**, 194101 (2006).

[28]Q. Wu and W. Yang, J. Chem. Phys. **116** (2002).

[29]S. Grimme, J. Comput. Chem. **27**, 1787 (2006).

[30]A. D. Becke, J. Chem. Phys. **107** (1997).

[31]L. A. Curtiss, K. Raghavachari, P. C. Redfern, and J. A. Pople, J. Chem. Phys. **106** (1997).

[32]A. J. Cohen, P. Mori-Sánchez, and W. Yang, Science **321**, 792 (2008).

[33]A. D. Becke and E. R. Johnson, J. Chem. Phys. **122**, 154104 (2005).

[34]E. R. Johnson and A. D. Becke, J. Chem. Phys. **123**, 024101 (2005).

[35]A. D. Becke and E. R. Johnson, J. Chem. Phys. **123**, 154101 (2005).

[36]A. D. Becke and E. R. Johnson, J. Chem. Phys. **124**, 014104 (2006).

[37]E. R. Johnson and A. D. Becke, J. Chem. Phys. **124**, 174104 (2006).

[38]A. D. Becke and E. R. Johnson, J. Chem. Phys. **127**, 154108 (2007).

[39]A. Otero-de-la Roza and E. R. Johnson, J. Chem. Phys. **138**, 204109 (2013).

[40]F. O. Kannemann and A. D. Becke, J. Chem. Theory Comput. **5**, 719 (2009).

[41]F. A. Gianturco and F. Paesani, Mol. Phys. **99**, 689 (2001).

[42]F. A. Gianturco, F. Paesani, M. F. Laranjeira, V. Vassilenko, and M. A. Cunha, J. Chem. Phys. **110** (1999).

[43]F. A. Gianturco and F. Paesani, J. Chem. Phys. **113**, 3011 (2000).

[44]Y. Andersson, D. C. Langreth, and B. I. Lundqvist, Phys. Rev. Lett. **76**, 102 (1996).

[45]M. Kamiya, T. Tsuneda, and K. Hirao, J. Chem. Phys. **117** (2002).

[46]T. Sato, T. Tsuneda, and K. Hirao, Mol. Phys. **103**, 1151 (2005).

[47]T. Schwabe and S. Grimme, Phys. Chem. Chem. Phys. **9**, 3397 (2007).

[48]P. Seal and S. Chakrabarti, J. Phys. Chem. A **113**, 1377 (2009).

[49]P. Seal, J. Comput. Chem. **31**, 2001 (2010).

[50]J. P. Perdew and K. Burke, Int. J. Quantum Chem. **57**, 309 (1996).

[51]A. D. Becke and M. R. Roussel, Phys. Rev. A **39**, 3761 (1989).

[52]F. Hirshfeld, Theor. Chim. Acta **44**, 129 (1977).

[53]R. G. Parr and W. Yang, *Density-Functional Theory of Atoms and Molecules* (Oxford University Press, New York, 1989).

[54]P. Hohenberg and W. Kohn, Phys. Rev. **136**, B864 (1964).

[55]W. Kohn and L. J. Sham, Phys. Rev. **140**, A1133 (1965).

[56]S. H. Vosko, L. Wilk, and M. Nusair, Can. J. Phys. **58**, 1200 (1980).

[57]J. P. Perdew and W. Yue, Phys. Rev. B **33**, 8800 (1986).

[58]A. D. Becke, Phys. Rev. A **38**, 3098 (1988).

[59]J. P. Perdew, J. A. Chevary, S. H. Vosko, K. A. Jackson, M. R. Pederson, D. J. Singh, and C. Fiolhais, Phys. Rev. B **46**, 6671 (1992).

[60]J. P. Perdew, K. Burke, and M. Ernzerhof, Phys. Rev. Lett. **77**, 3865 (1996).

[61]D. J. Lacks and R. G. Gordon, Phys. Rev. A **47**, 4681 (1993).

[62]J. P. Perdew, K. Burke, and Y. Wang, Phys. Rev. B **54**, 16533 (1996).

[63]C. Lee, W. Yang, and R. G. Parr, Phys. Rev. B **37**, 785 (1988).

[64]J. P. Perdew and Y. Wang, Phys. Rev. B **45**, 13244 (1992).

[65]F. O. Kannemann and A. D. Becke, J. Chem. Theory Comput. **6**, 1081 (2010).

[66]A. Otero-de-la Roza and E. R. Johnson, J. Chem. Phys. **136**, 174109 (2012).

[67]E. J. Baerends and O. V. Gritsenko, J. Phys. Chem. A **101**, 5383 (1997).

[68]A. D. Becke, J. Chem. Phys. **98** (1993).

[69]L. A. Curtiss, K. Raghavachari, P. C. Redfern, and J. A. Pople, J. Chem. Phys. **112** (2000).

[70]M. J. Frisch, G. W. Trucks, H. B. Schlegel, G. E. Scuseria, M. A. Robb, J. R. Cheeseman, G. Scalmani, V. Barone, B. Mennucci, G. A. Petersson, H. Nakatsuji, M. Caricato, X. Li, H. P. Hratchian, A. F. Izmaylov, J. Bloino, G. Zheng, J. L.

Sonnenberg, M. Hada, M. Ehara, K. Toyota, R. Fukuda, J. Hasegawa, M. Ishida, T. Nakajima, Y. Honda, O. Kitao, H. Nakai, T. Vreven, J. A. Montgomery, Jr., J. E. Peralta, F. Ogliaro, M. Bearpark, J. J. Heyd, E. Brothers, K. N. Kudin, V. N. Staroverov, R. Kobayashi, J. Normand, K. Raghavachari, A. Rendell, J. C. Burant, S. S. Iyengar, J. Tomasi, M. Cossi, N. Rega, J. M. Millam, M. Klene, J. E. Knox, J. B. Cross, V. Bakken, C. Adamo, J. Jaramillo, R. Gomperts, R. E. Stratmann, O. Yazyev, A. J. Austin, R. Cammi, C. Pomelli, J. W. Ochterski, R. L. Martin, K. Morokuma, V. G. Zakrzewski, G. A. Voth, P. Salvador, J. J. Dannenberg, S. Dapprich, A. D. Daniels, O. Farkas, J. B. Foresman, J. V. Ortiz, J. Cioslowski, and D. J. Fox, "Gaussian 09 Revision B.01," Gaussian Inc. Wallingford CT 2010.

[71]E. R. Johnson, R. A. Wolkow, and G. A. DiLabio, Chem. Phys. Lett. **394**, 334 (2004).

[72]E. R. Johnson, A. D. Becke, C. D. Sherrill, and G. A. DiLabio, J. Chem. Phys. **131**, 034111 (2009).

[73]D. E. Woon and T. H. Dunning, J. Chem. Phys. **100** (1994).

[74]C. Zhang, Z. Wang, and E. Feng, Chem. Phys. Lett. **517**, 16 (2011).

[75]Z. Wang, E. Feng, H. Yu, C. Zhang, and J. Du, J. Chem. Phys. **134**, 024320 (2011).

[76]R. R. Toczyłowski and S. M. Cybulski, J. Chem. Phys. **112** (2000).

[77]H. Ran and D. Xie, J. Chem. Phys. **128**, 124323 (2008).

[78]R. Chen, E. Jiao, H. Zhu, and D. Xie, J. Chem. Phys. **133**, 104302 (2010).

[79]R. Chen, H. Zhu, and D. Xie, Chem. Phys. Lett. **511**, 229 (2011).

[80]C. Sun, Z. Wang, E. Feng, and C. Zhang, Chem. Phys. Lett. **592**, 182 (2014).

[81]C. Sun, X. Shao, C. Yu, E. Feng, and W. Huang, Chem. Phys. Lett. **549**, 12 (2012).

[82]MATLAB, *version 8.1.0.604 (R2013a)* (The MathWorks Inc., Natick, Massachusetts, 2013).

[83]C. R. Munteanu, J. L. Cacheiro, and B. Fernández, J. Chem. Phys. **121**, 9104 (2004).

[84]C. R. Munteanu and B. Fernández, J. Chem. Phys. **123**, 014309 (2005).

[85]C. R. Munteanu, J. L. Cacheiro, and B. Fernández, J. Chem. Phys. **120**, 9104 (2004).

[86]H. Zhu, Y. Zhou, and D. Xie, J. Chem. Phys. **122**, 234312 (2005).

[87]H. Zhu, Y. Guo, Y. Xue, and D. Xie, J. Comput. Chem. **27**, 1045 (2006).

[88]E. Feng, C. Sun, C. Yu, X. Shao, and W. Huang, J. Chem. Phys. **135**, 124301 (2011).

[89]F. Lique, Chem. Phys. Lett. **471**, 54 (2009).

[90]Y. Zhou and D. Xie, J. Chem. Phys. **123**, 134323 (2005).

[91]K. Peterson and G. McBane, J. Chem. Phys. **123**, 084314 (2005).

[92]E. Feng, Z. Wang, M. Gong, and Z. Cui, J. Chem. Phys. **127**, 174301 (2007).

[93]R. G. A. Bone, J. Phys. Chem. **98**, 3126 (1994).

[94]C. Lauzin, E. Cauët, J. Demaison, M. Herman, H. Stoll, and J. Liévin, Mol. Phys. **110**, 2751 (2012).

[95]R. R. Toczyłowski, F. Doloresco, and S. M. Cybulski, J. Chem. Phys. **114** (2001).

[96]Z. Wang, C. Zhang, E. Feng, H. Yu, and J. Du, Chem. Phys. Lett. **501**, 206 (2011).

[97]J. L. Cagide Fajín and B. Fernández, Chem. Phys. Lett. **419**, 55 (2006).

[98]J. L. Cagide Fajín, J. Lopez Cacheiro, and B. Fernández, J. Chem. Phys. **121**, 4599 (2004).

[99]P. Slavíček, M. Roeselová, P. Jungwirth, and B. Schmidt, J. Chem. Phys. **114**, 1539 (2001).

[100]J. L. Cagide Fajín, B. Fernández, A. Mikosz, and D. Farrelly, Mol. Phys **104**, 1413 (2006).

[101]C. Zhang, Z. Wang, H. Yu, J. Du, and J. Ma, Chem. Phys. Lett. **495**, 166 (2010).

[102]A. Tulegenov, R. Wheatley, and M. Nauryzbaev, Chem. Phys. Lett. **468**, 290 (2009).

Appendix A: Additional information for the vdW molecules

FIG. A.1. Jacobi coordinates for the remaining vdW complexes.

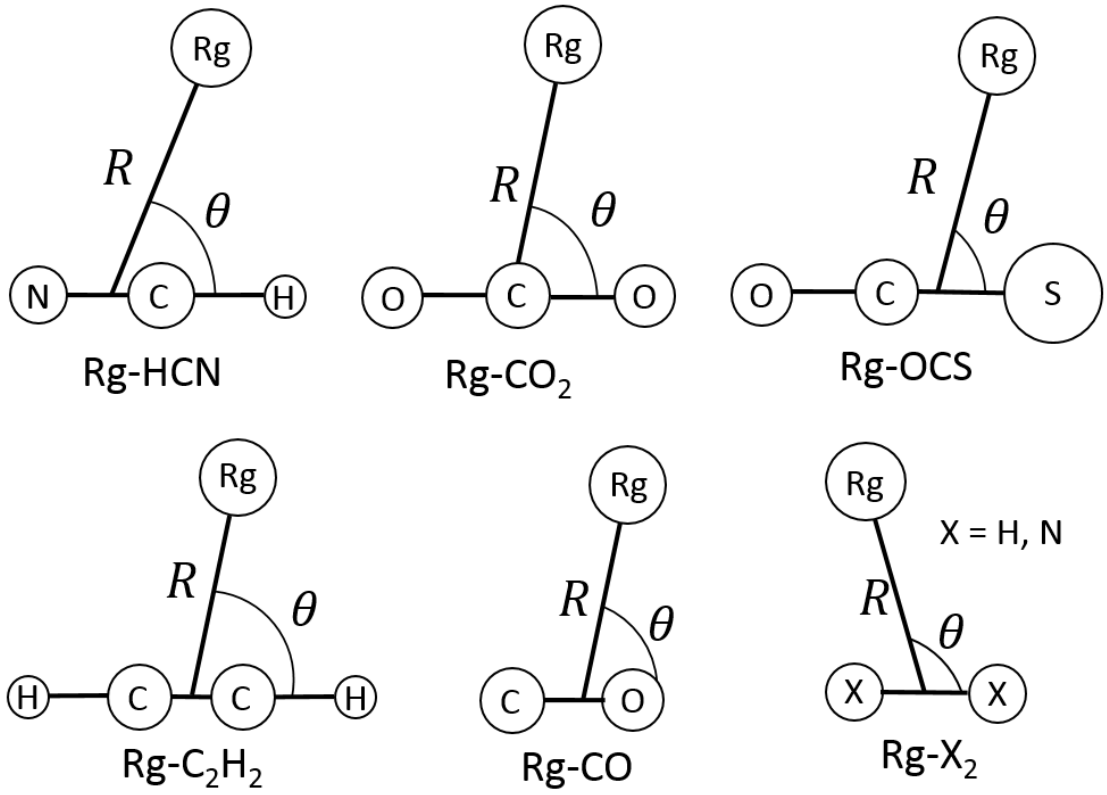

TABLE A.1 Optimized bond lengths of linear molecules with respect to the center of mass as the origin in Å with dispersion-corrected functionals.

Molecule	**Bond**	**HFPBE**	**PW86PBE**	**PW1PBE**	**B97-D**
CO	C-X	0.6248	0.6488	0.6434	0.6470
	O-X	0.4686	0.4866	0.4826	0.4853
H_2	H-X	0.3653	0.3731	0.3715	0.3719
N_2	N-X	0.5291	0.5511	0.5463	0.5489
HF	H-X	0.7997	0.8385	0.8302	0.8317
	F-X	0.0889	0.0932	0.0922	0.0924
HCl	H-X	1.1839	1.2177	1.2098	1.2098
	Cl-X	0.0696	0.0716	0.0712	0.0712
HBr	H-X	1.3539	1.3953	1.3861	1.3856
	Br-X	0.0387	0.0399	0.0396	0.0396
CO_2	C-O	1.1246	1.1717	1.1609	1.1669
OCS	O-X	1.6389	1.6955	1.6825	1.6899
	C-X	0.5241	0.5267	0.5256	0.5254
	S-X	1.0160	1.0452	1.0383	1.0420
HCN	H-X	1.5341	1.5748	1.5657	1.5723
	C-X	0.4826	0.5021	0.4978	0.5008
	N-X	0.6328	0.6553	0.6504	0.6539
C_2H_2	C-X	0.5853	0.6030	0.5992	0.6023
	H-X	1.6338	1.6713	1.6631	1.6694

TABLE A.2 Bond length and angle increments for Jacobi coordinates used to compute the PES of vdW molecules.

Rg	**Molecule**	**R**		$\boldsymbol{\theta}$	
		Range	Increment	Range	Increment
Ne	H_2	4.00-5.40 a_0	0.20 a_0	0-90°	10°
		5.50-7.30 a_0	0.05 a_0		
		7.40-7.50 a_0	0.10 a_0		
		7.70-9.50 a_0	0.20 a_0		
Kr	H_2	3.00-4.50 Å	0.05 Å	0-90°	10°
		4.60-5.00 Å	0.10 Å		
		5.20-6.00 Å	0.20 Å		
Ne	N_2	3.00-4.50 Å	0.05 Å	0-60°	10°
		4.60-4.70 Å	0.10 Å	65-90°	5°
		4.80-5.00 Å	0.20 Å		
Ar	N_2	3.20-4.50 Å	0.05 Å	0-60°	10°
		4.60-4.70 Å	0.10 Å	65-90°	5°
		4.80-5.00 Å	0.20 Å		
Kr	N_2	6.00-6.50 a_0	0.10 a_0	0-60°	10°
		6.55-9.00 a_0	0.05 a_0	65-90°	5°
		9.10-9.90 a_0	0.10 a_0		
He	CO	6.00-6.50 a_0	0.10 a_0	0-60°	10°
		6.55-9.00 a_0	0.05 a_0	70-105°	5°
		9.10-9.90 a_0	0.10 a_0	115-135°	10°
				150-180°	15°
Ne	CO	5.00-7.40 a_0	0.05 a_0	0-60°	10°

TABLE A.2 – Continued

Rg	**Molecule**	**R**		$\boldsymbol{\theta}$	
		Range	Increment	Range	Increment
		7.50-8.10 a_0	0.10 a_0	75-105°	5°
		8.30-9.50 a_0	0.20 a_0	115-125°	10°
				135-180°	15°
Ar	CO	3.20-4.50 Å	0.05 Å	0-60°	10°
		4.60-5.30 Å	0.10 Å	75-105°	5°
		5.50-6.10 Å	0.20 Å	115-125°	10°
		6.15-6.30 Å	0.10 Å	135-180°	15°
		6.50 Å			
Kr	CO	6.00-8.00 a_0	0.05 a_0	0-60°	10°
		8.10-8.20 a_0	0.10 a_0	75-125°	5°
		8.40-10.00 a_0	0.20 a_0	135-165°	10°
				170-180°	10°
He	HF	2.60-4.30 Å	0.05 Å	0-80°	20°
		4.40-5.00 Å	0.10 Å	105-135°	10°
		5.20-5.60 Å	0.20 Å	150-180°	15°
		5.05 Å			
Kr	HF	5.70-6.00 a_0	0.10 a_0	0-180°	15°
		6.05-7.45 a_0	0.05 a_0		
		7.50-7.70 a_0	0.10 a_0		
		7.90-9.50 a_0	0.20 a_0		
He	HCl	3.00-4.50 Å	0.05 Å	0-180°	15°
		4.60-5.00 Å	0.10 Å		

TABLE A.2 – Continued

Rg	**Molecule**	**R**		$\boldsymbol{\theta}$	
		Range	Increment	Range	Increment
Ne	HCl	3.00-4.20 Å	0.05 Å	0-180°	15°
		4.30-5.00 Å	0.10 Å		
Ne	HBr	3.00-5.00 Å	0.05 Å	0-180°	15°
		5.10-5.50 Å	0.10 Å		
He	CO_2	4.50-5.00 a_0	0.10 a_0	0-90°	5°
		5.05-9.00 a_0	0.05 a_0		
		9.10-10.00 a_0	0.10 a_0		
Ne	CO_2	5.00-9.00 a_0	0.05 a_0	15-90°	5°
		9.10-10.00 a_0	0.10 a_0	0°	
		10.20-12.00 a_0	0.20 a_0		
Kr	CO_2	5.60-9.30 a_0	0.05 a_0	15-90°	5°
		9.40-10.20 a_0	0.10 a_0	0°	
		10.40-13.00 a_0	0.20 a_0		
Ne	OCS	2.80-3.00 Å	0.10 Å	0-20°	5°
		3.10-5.30 Å	0.05 Å	30-160°	5°
		5.40-6.00 Å	0.10 Å	165-180°	15°
		6.20-7.00 Å	0.20 Å		
Ar	OCS	3.10-3.20 Å	0.10 Å	0-20°	5°
		3.25-5.10 Å	0.05 Å	30-160°	5°
		5.20-5.40 Å	0.10 Å	165-180°	15°
		5.60-6.00 Å	0.20 Å		
Kr	OCS	6.00-10.00 a_0	0.05 a_0	0-40°	20°

TABLE A.2 – Continued

Rg	**Molecule**	**R**		$\boldsymbol{\theta}$	
		Range	Increment	Range	Increment
		10.10-10.20 a_0	0.10 a_0	50-135°	5°
		10.40-11.00 a_0	0.20 a_0	150-170°	20°
				180°	
He	HCN	6.00-9.00 a_0	0.05 a_0	0-130°	5°
		9.10-9.60 a_0	0.10 a_0	140-180°	10°
		9.80-10.00 a_0	0.20 a_0		
Ne	HCN	6.00-9.00 a_0	0.05 a_0	0-110°	5°
		9.10-9.60 a_0	0.10 a_0	120-180°	10°
		9.80-10.00 a_0	0.20 a_0		
Ar	HCN	6.00-9.50 a_0	0.05 a_0	0-110°	5°
		9.60-10.00 a_0	0.20 a_0	120-180°	10°
Kr	HCN	6.00-9.50 a_0	0.05 a_0	0-120°	5°
		9.60-10.00 a_0	0.20 a_0	130-180°	10°
He	C_2H_2	3.00-5.50 Å	0.05 Å	0-90°	5°
Ne	C_2H_2	3.10-5.00 Å	0.05 Å	0-90°	5°
Ar	C_2H_2	3.50-5.00 Å	0.05 Å	0-90°	5°
Kr	C_2H_2	3.50-5.50 Å	0.05 Å	0-90°	5°

Appendix B: PES of other Rg-linear molecule vdW complexes

FIG. B.1. PES of Ne-H_2 with XDM-corrected functionals and B97-D.

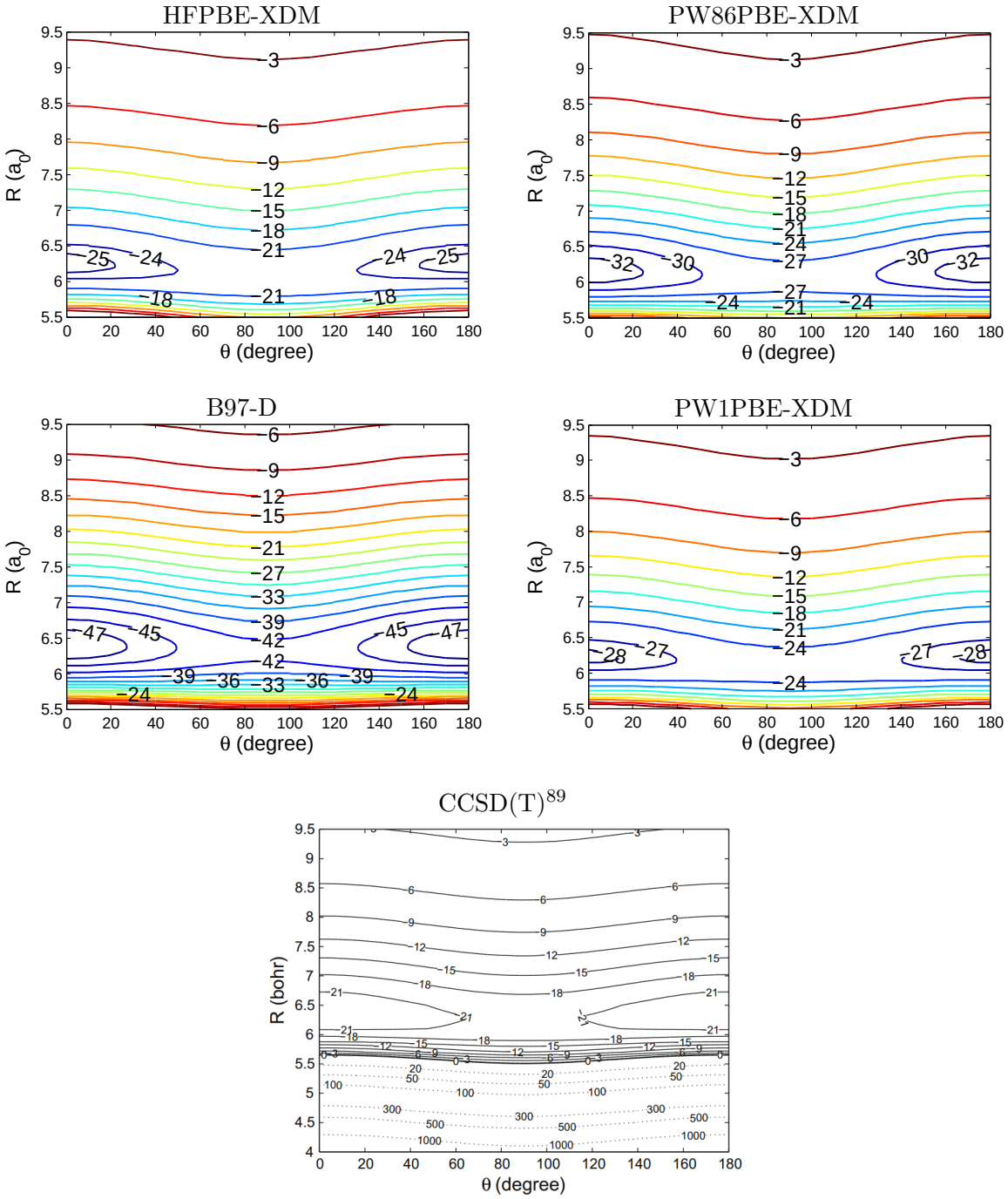

FIG. B.2. PES of Kr-H_2 with XDM-corrected functionals and B97-D. The reference PES did not use bond length of H_2.

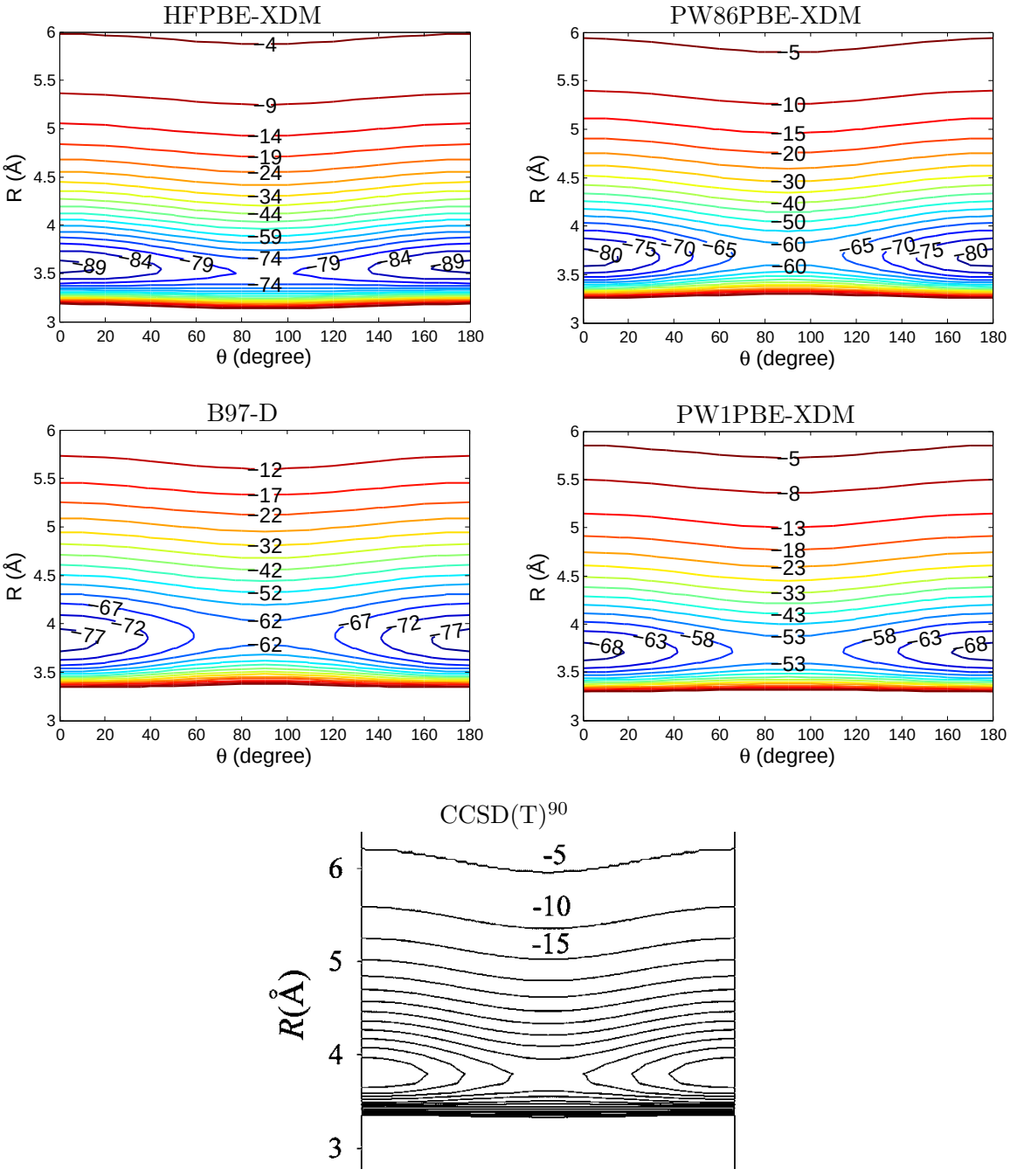

FIG. B.3. PES of Ne-N_2 with XDM-corrected functionals and B97-D. The global minimum from the reference PES is labeled as 0 cm^{-1}.

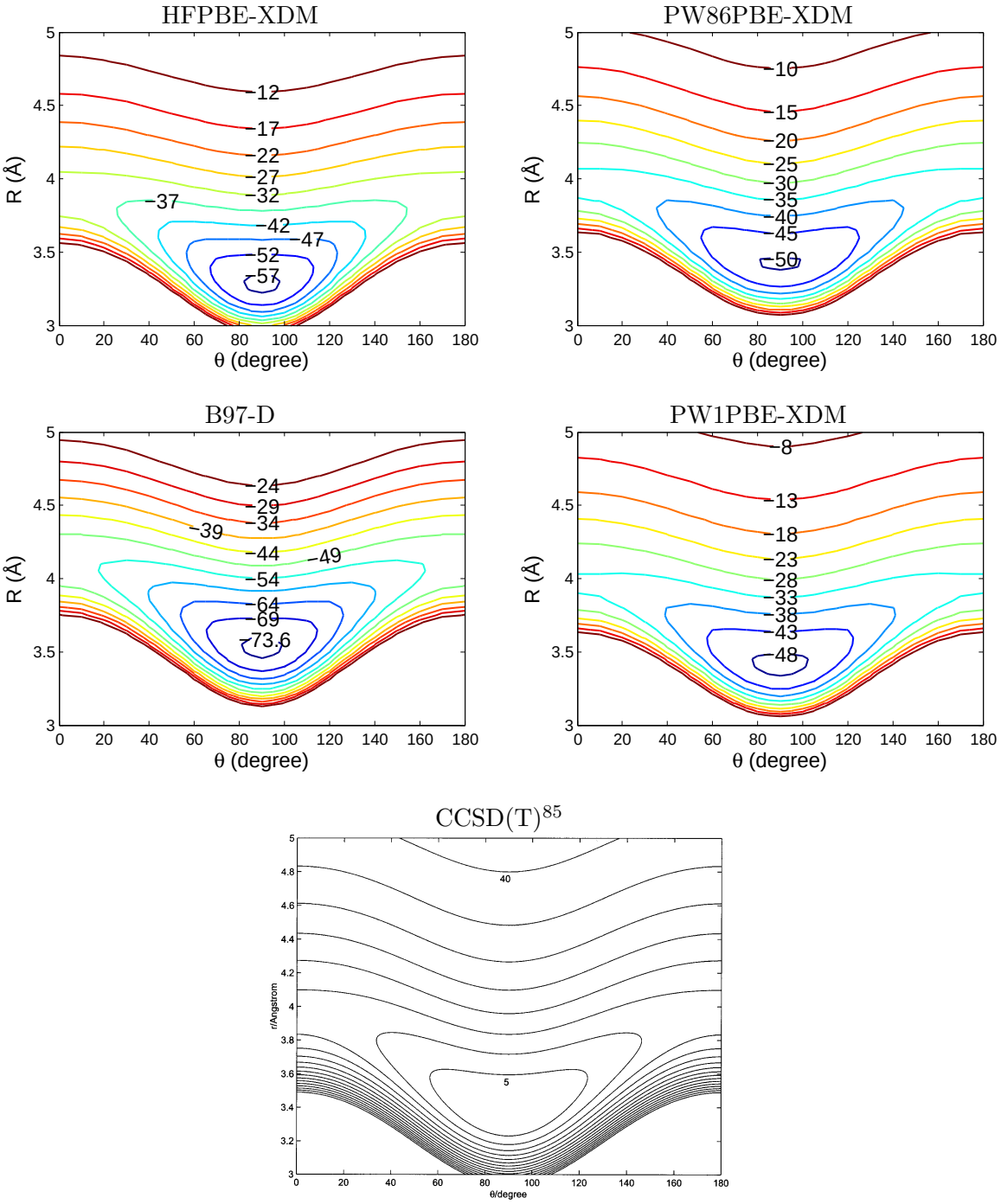

FIG. B.4. PES of Kr-N_2 with XDM-corrected functionals and B97-D. Only the half portion of the reference PES is shown and the bond angle is aligned at the vertical axis.

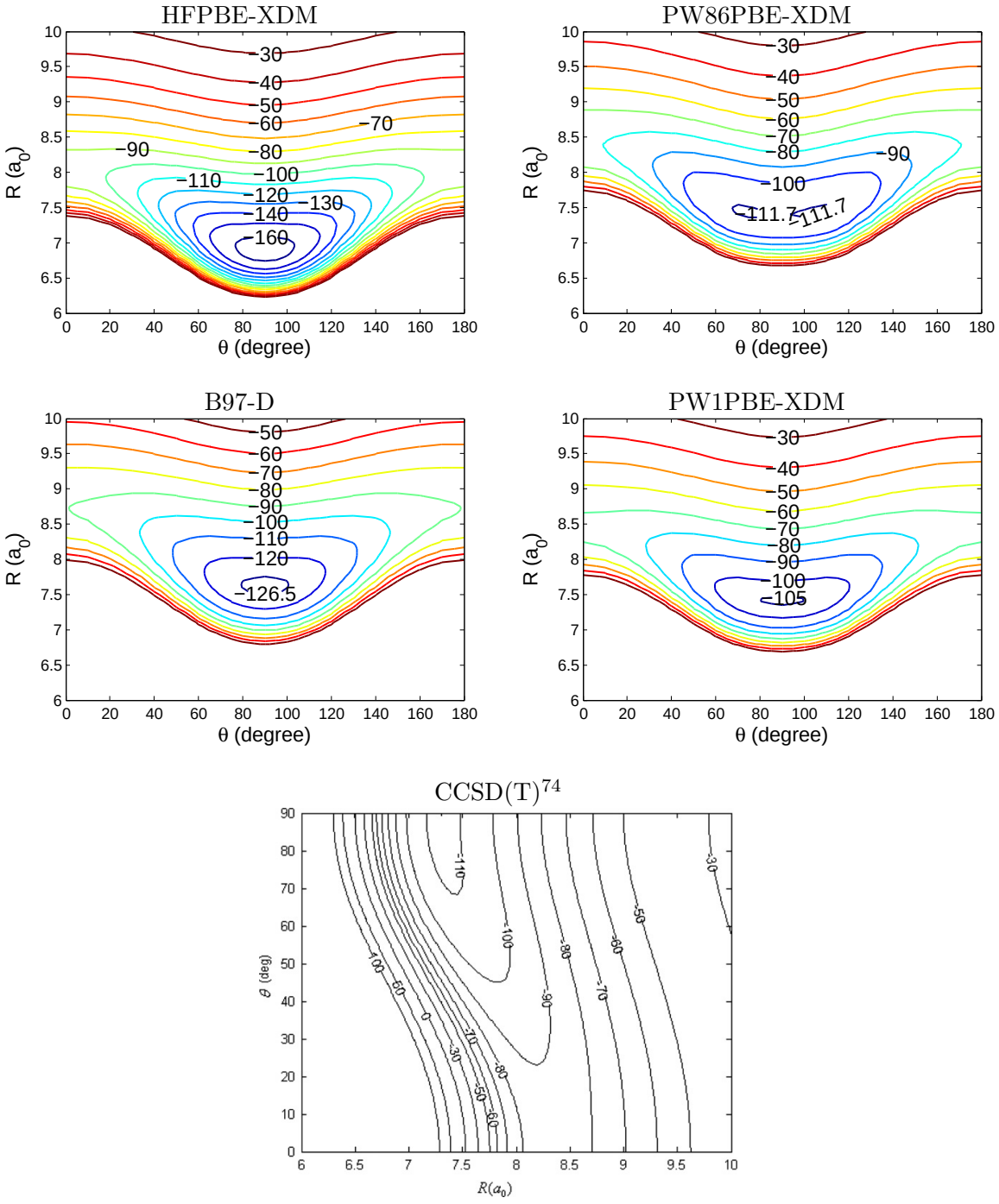

FIG. B.5. PES of He-CO with XDM-corrected functionals and B97-D.

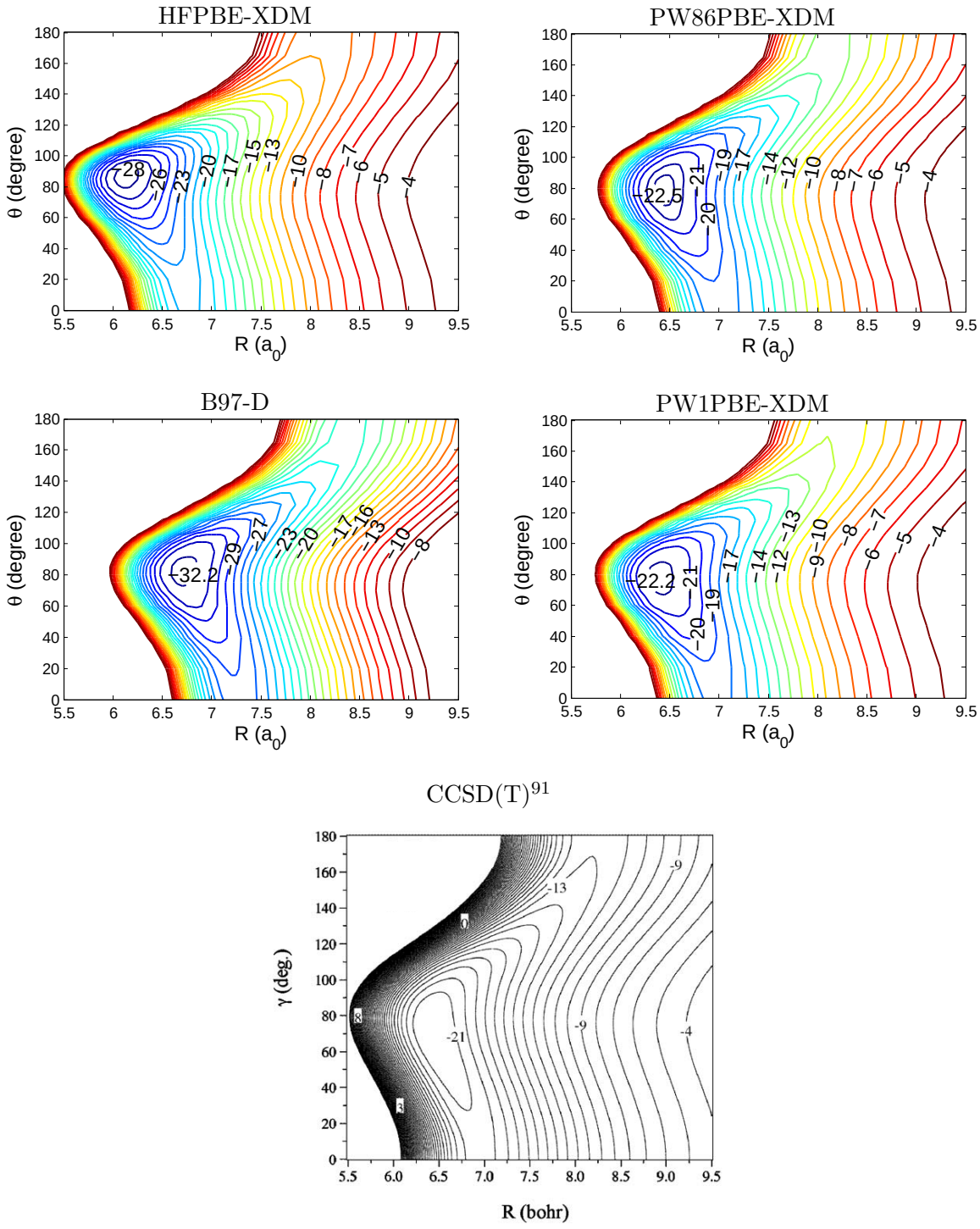

FIG. B.6. PES of Ne-CO with XDM-corrected functionals and B97-D.

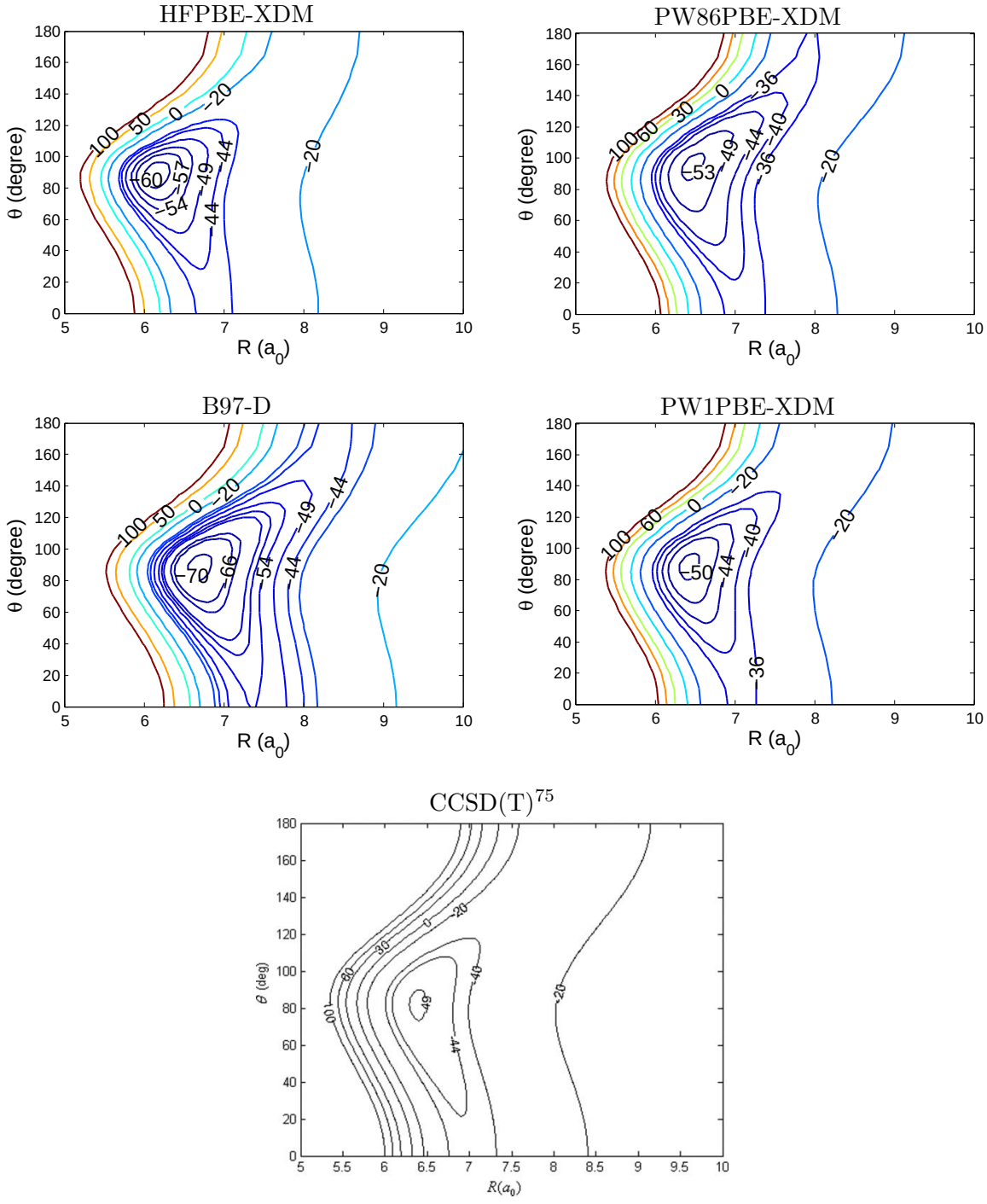

FIG. B.7. PES of Ar-CO with XDM-corrected functionals and B97-D.

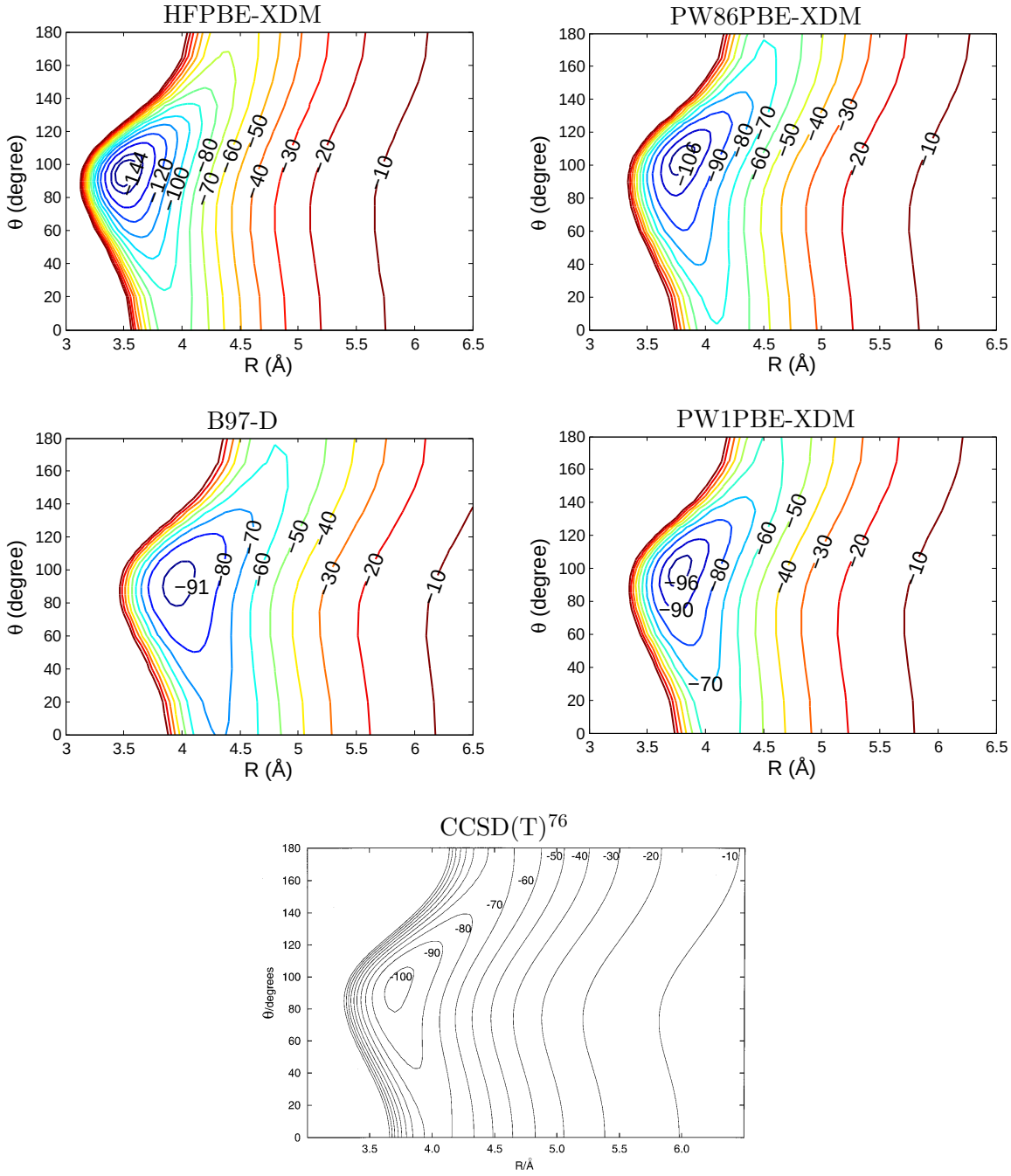

FIG. B.8. PES of Kr-CO with XDM-corrected functionals and B97-D.

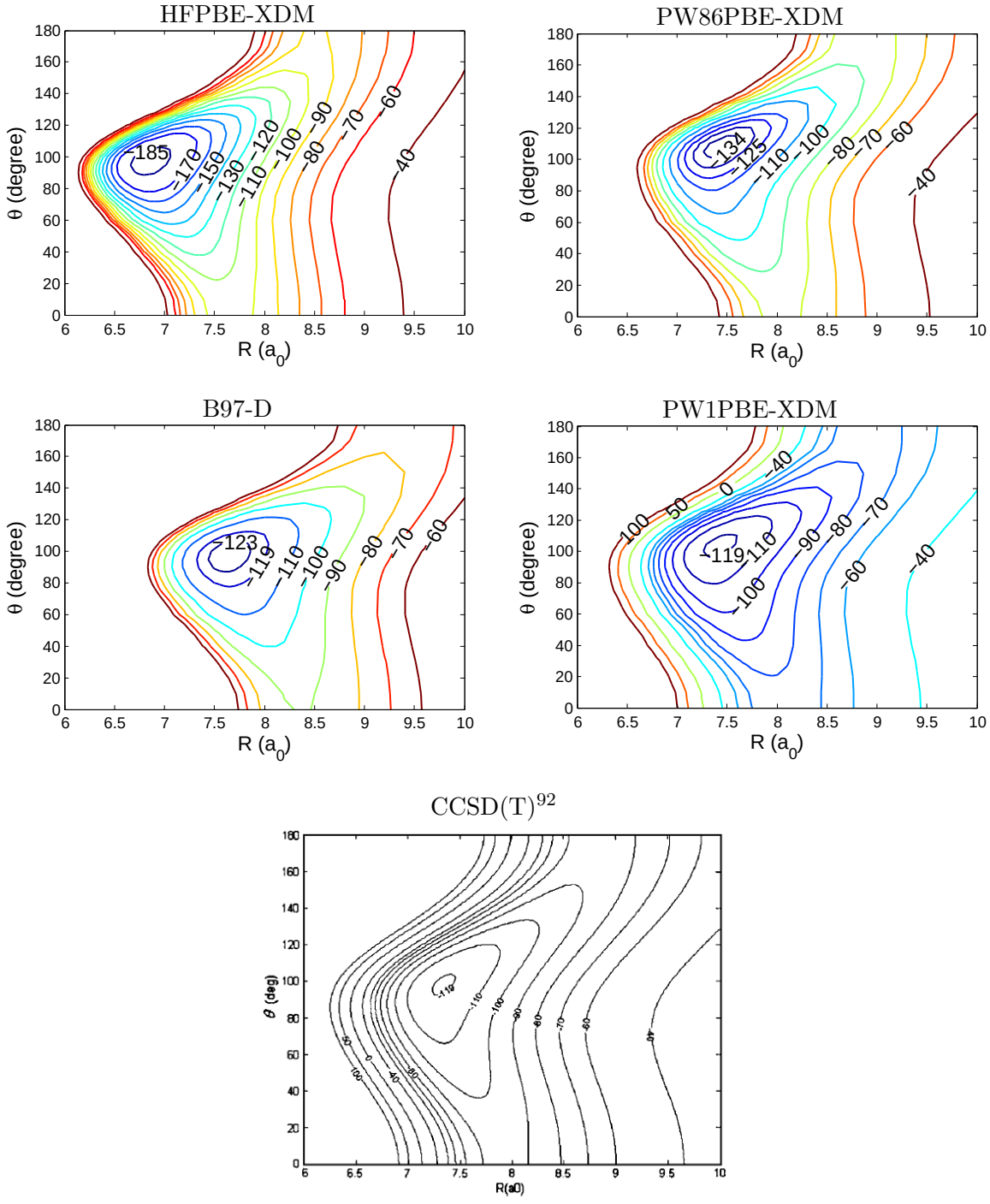

FIG. B.9. PES of He-HF with XDM-corrected functionals and B97-D.

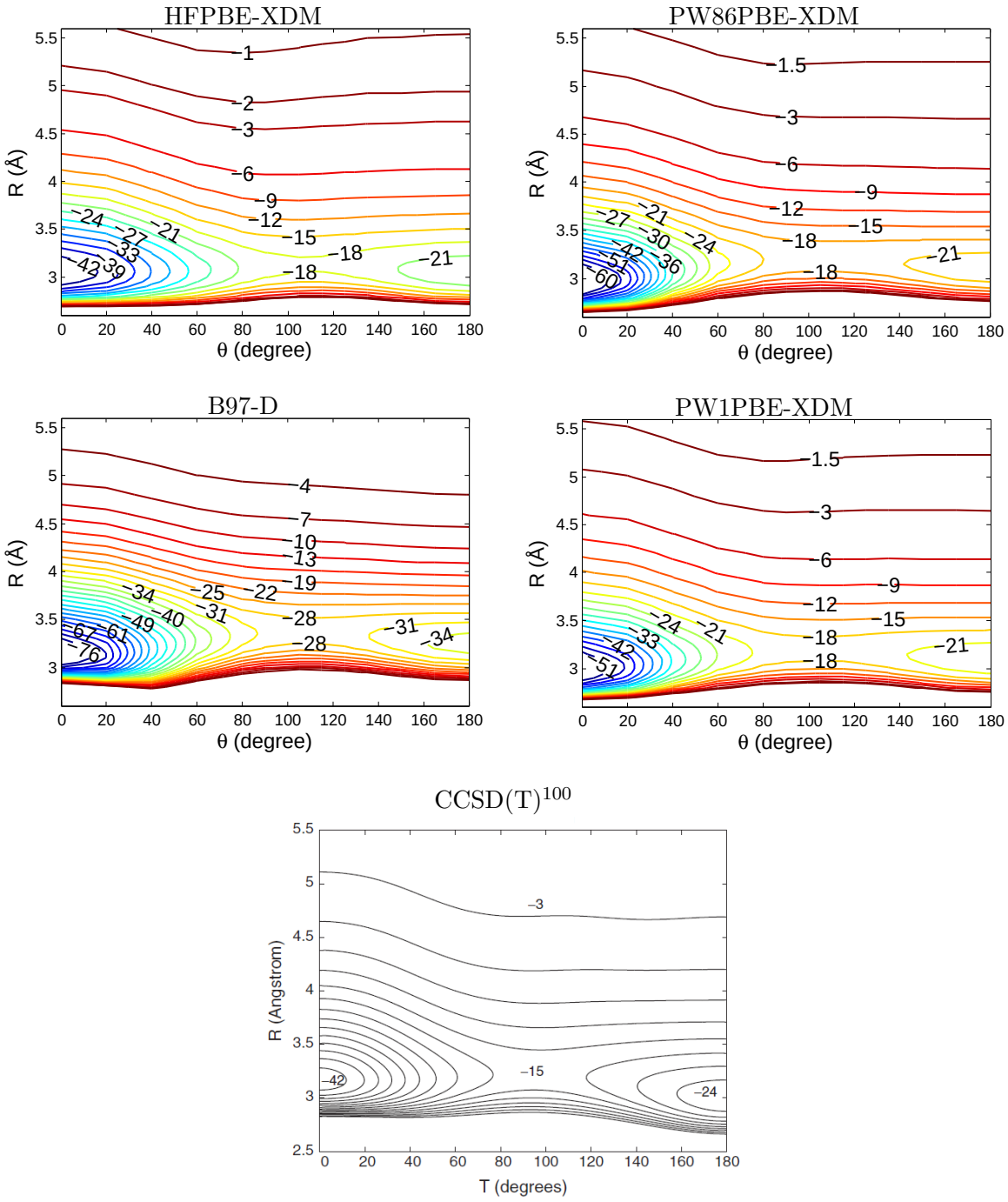

FIG. B.10. PES of He-HCl with XDM-corrected functionals and B97-D.

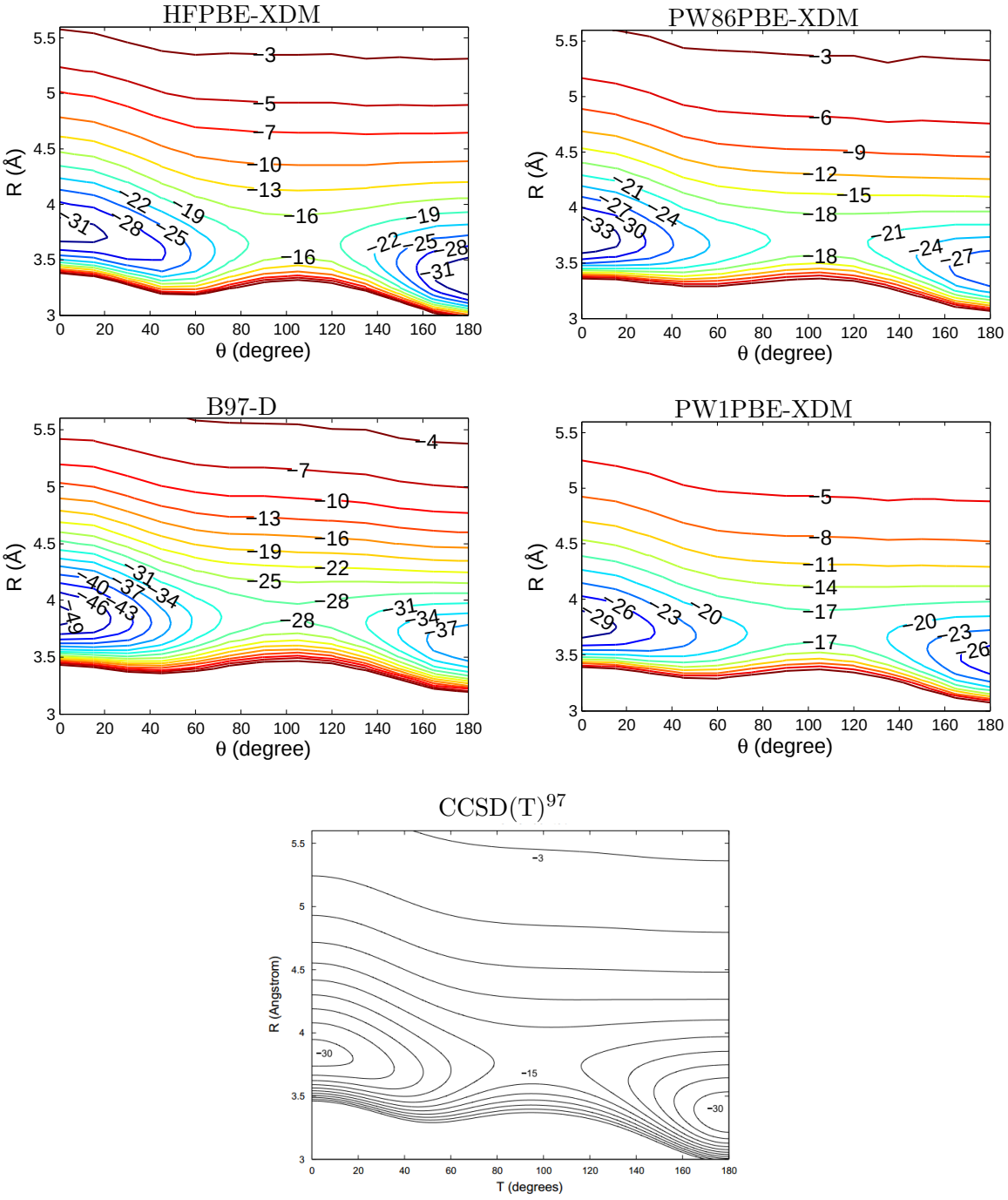

FIG. B.11. PES of Ne-HCl with XDM-corrected functionals and B97-D. The bond angle is aligned at the vertical axis of the reference PES.

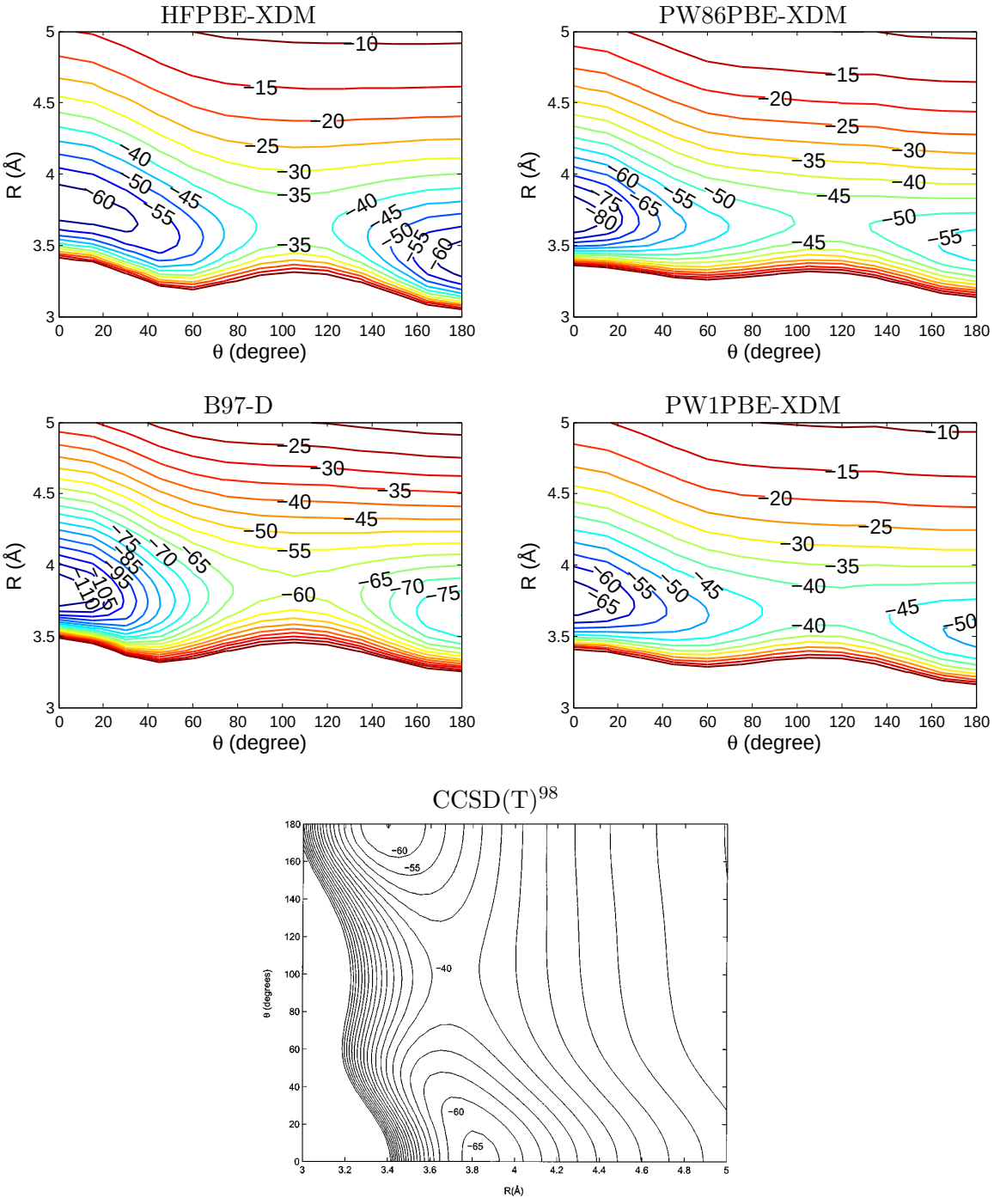

FIG. B.12. PES of Ne-HBr with XDM-corrected functionals and B97-D. The bond angle is aligned at the vertical axis of the reference PES.

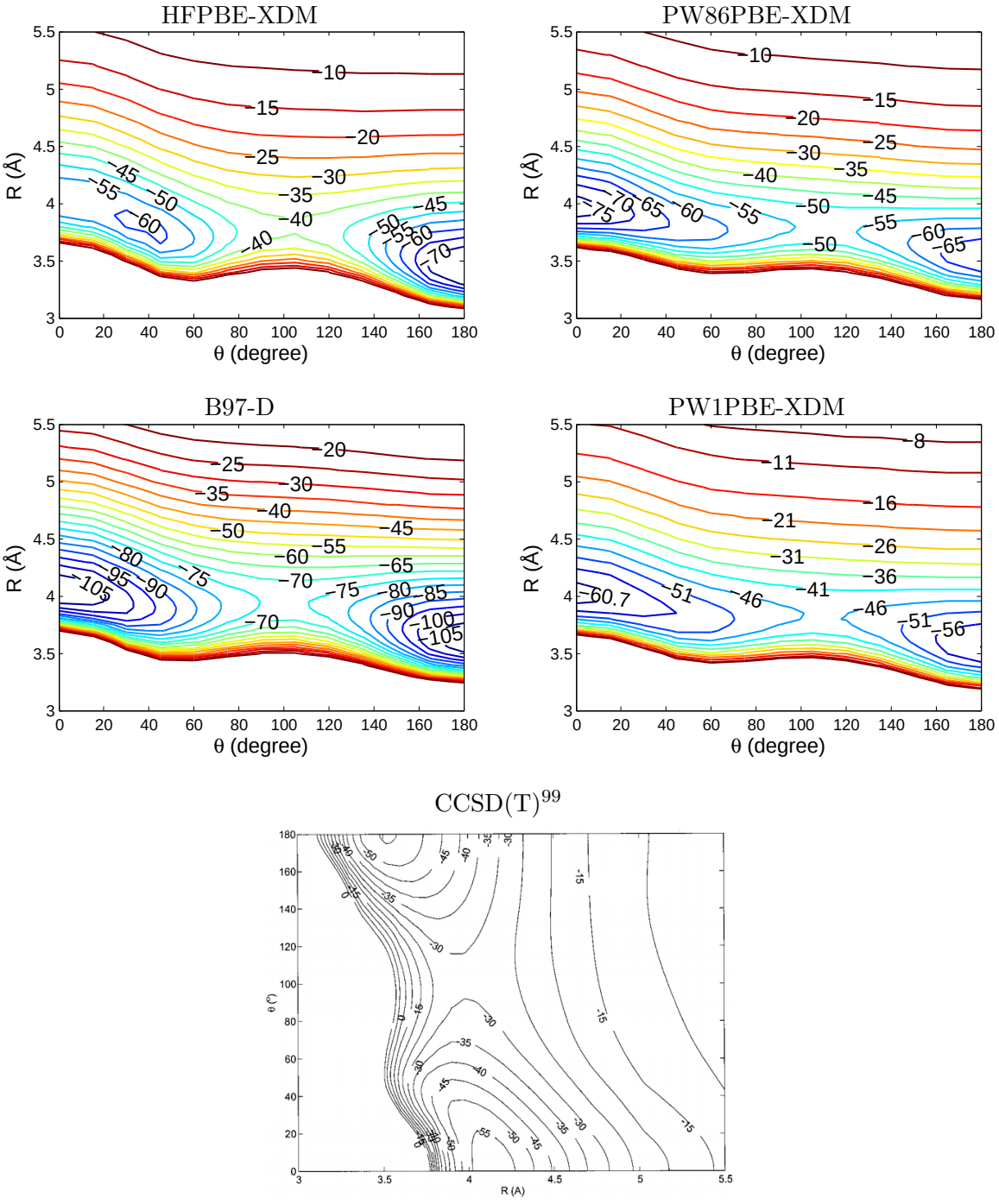

FIG. B.13. PES of He-CO_2 with XDM-corrected functionals and B97-D. The contours of the reference PES are in increments of 5 cm^{-1}.

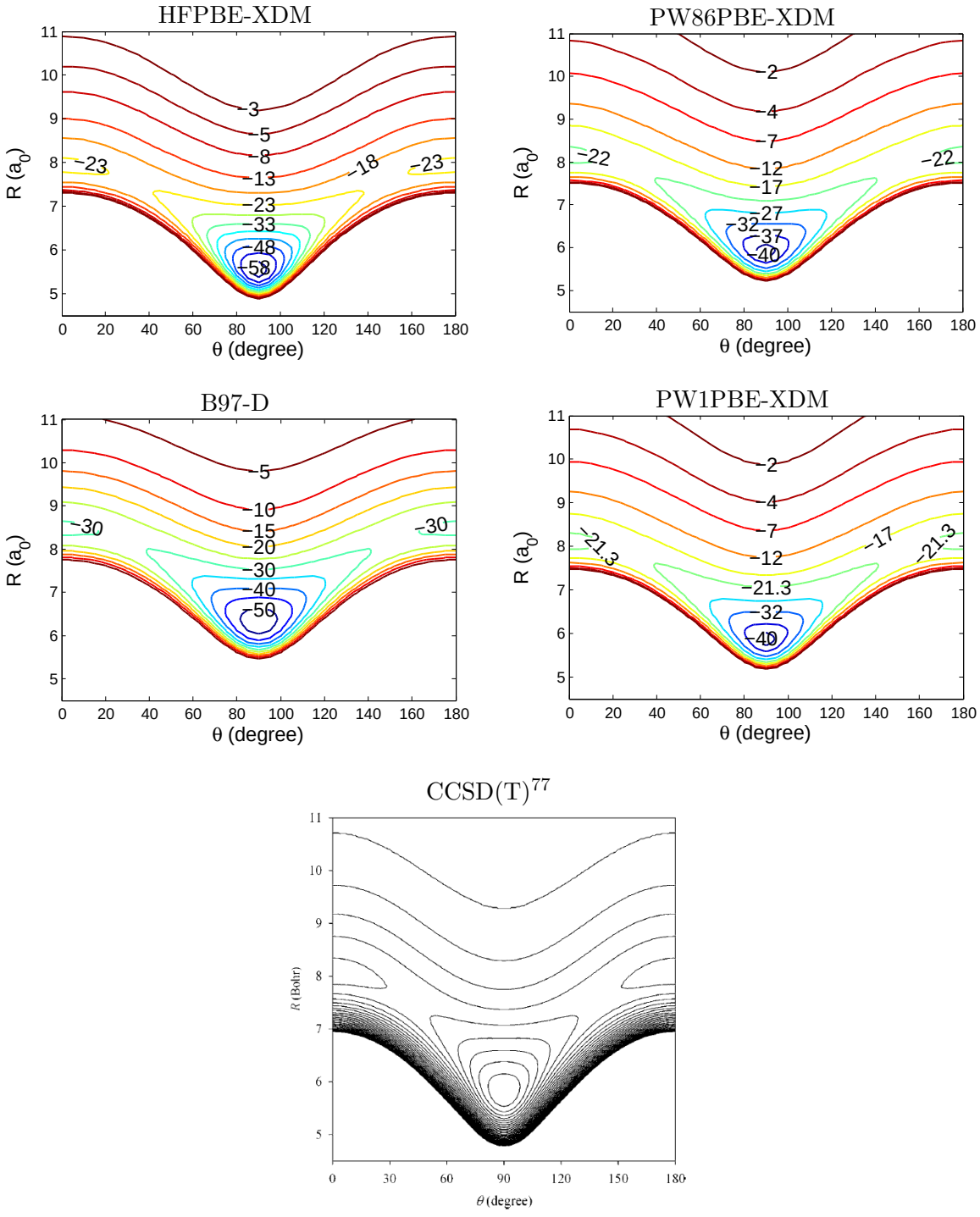

FIG. B.14. PES of Ne-CO_2 with XDM-corrected functionals and B97-D. The contours of the reference PES are in increments of 5 cm^{-1}.

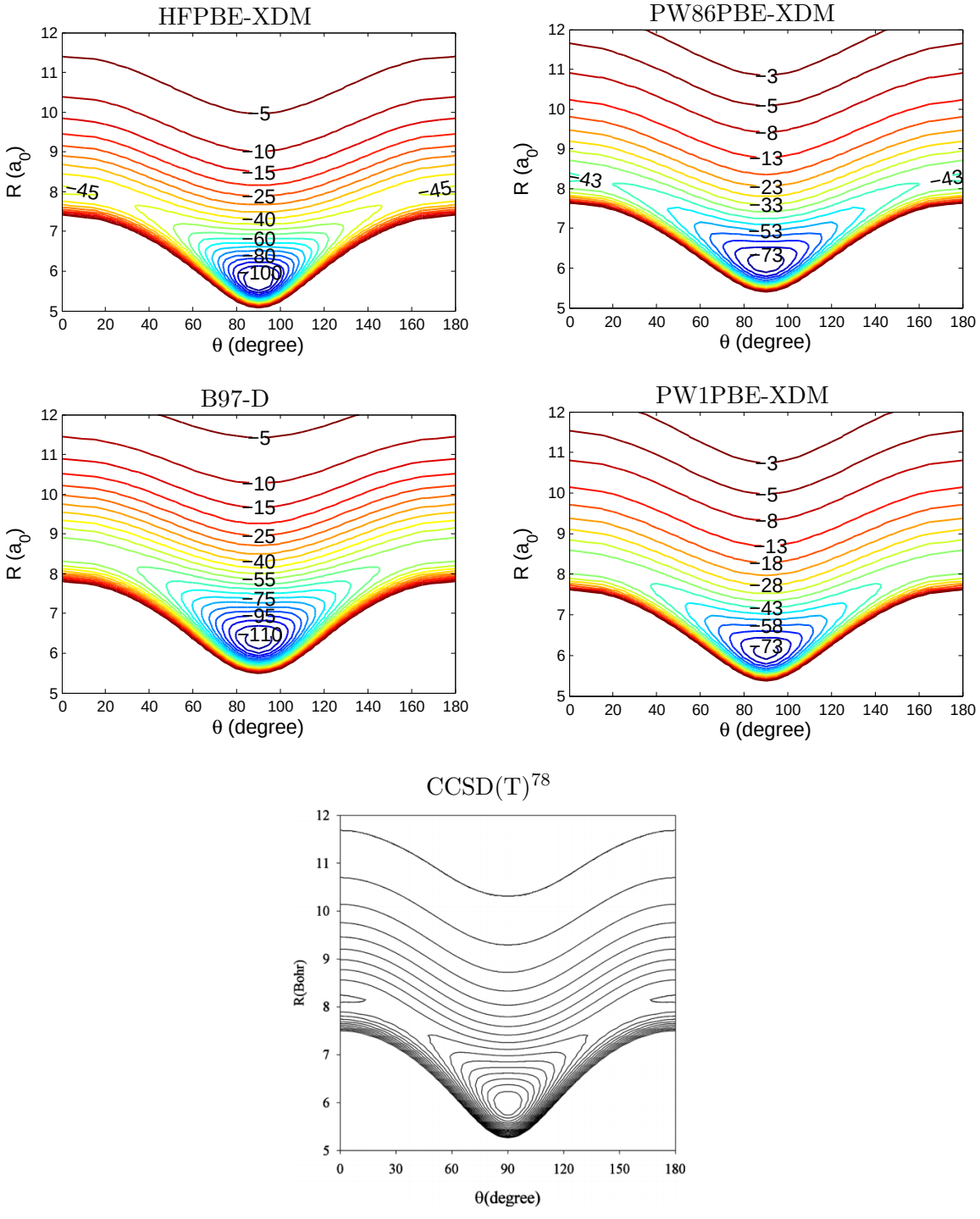

FIG. B.15. PES of Kr-CO_2 with XDM-corrected functionals and B97-D. The contours of the reference PES are in increments of 10 cm^{-1}.

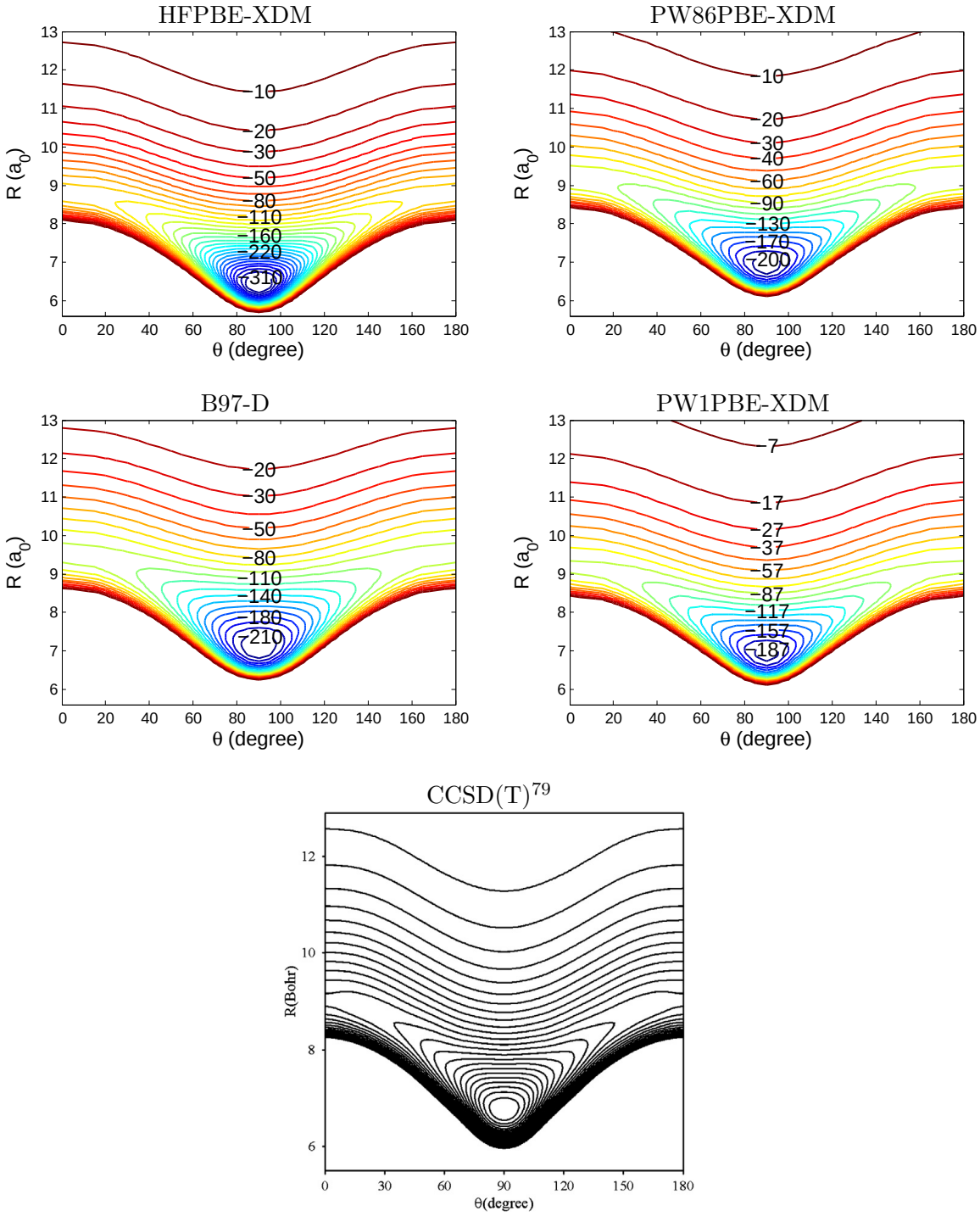

FIG. B.16. PES of Ne-OCS with XDM-corrected functionals and B97-D. The reference PES defines the angle $\theta = 0°$ at the Ne-O-C-S arrangement and the bond length is aligned at the vertical axis.

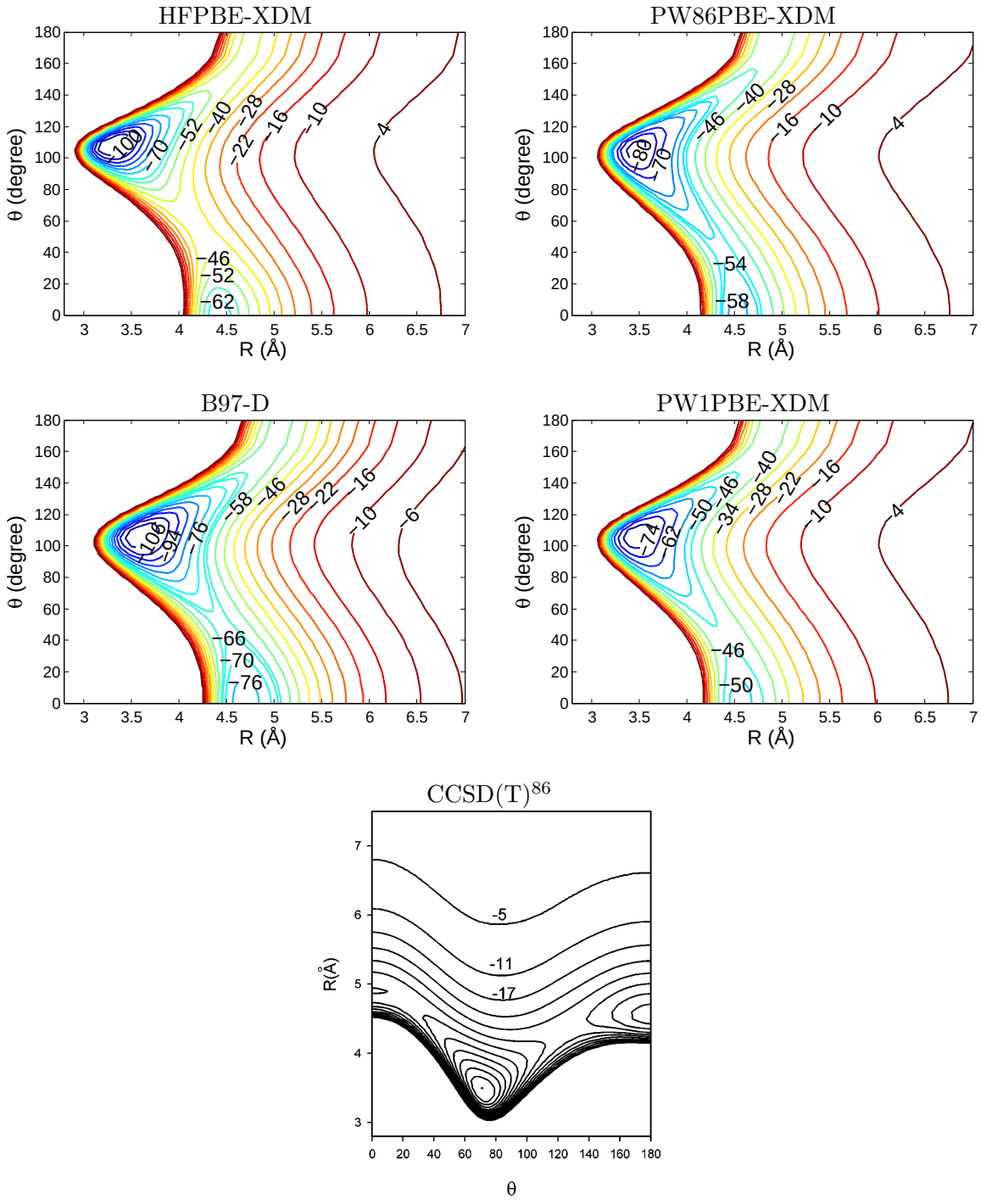

FIG. B.17. PES of Ar-OCS with XDM-corrected functionals and B97-D. The reference PES defines the angle $\theta = 0°$ at the Ar-O-C-S arrangement and the bond length is aligned at the vertical axis.

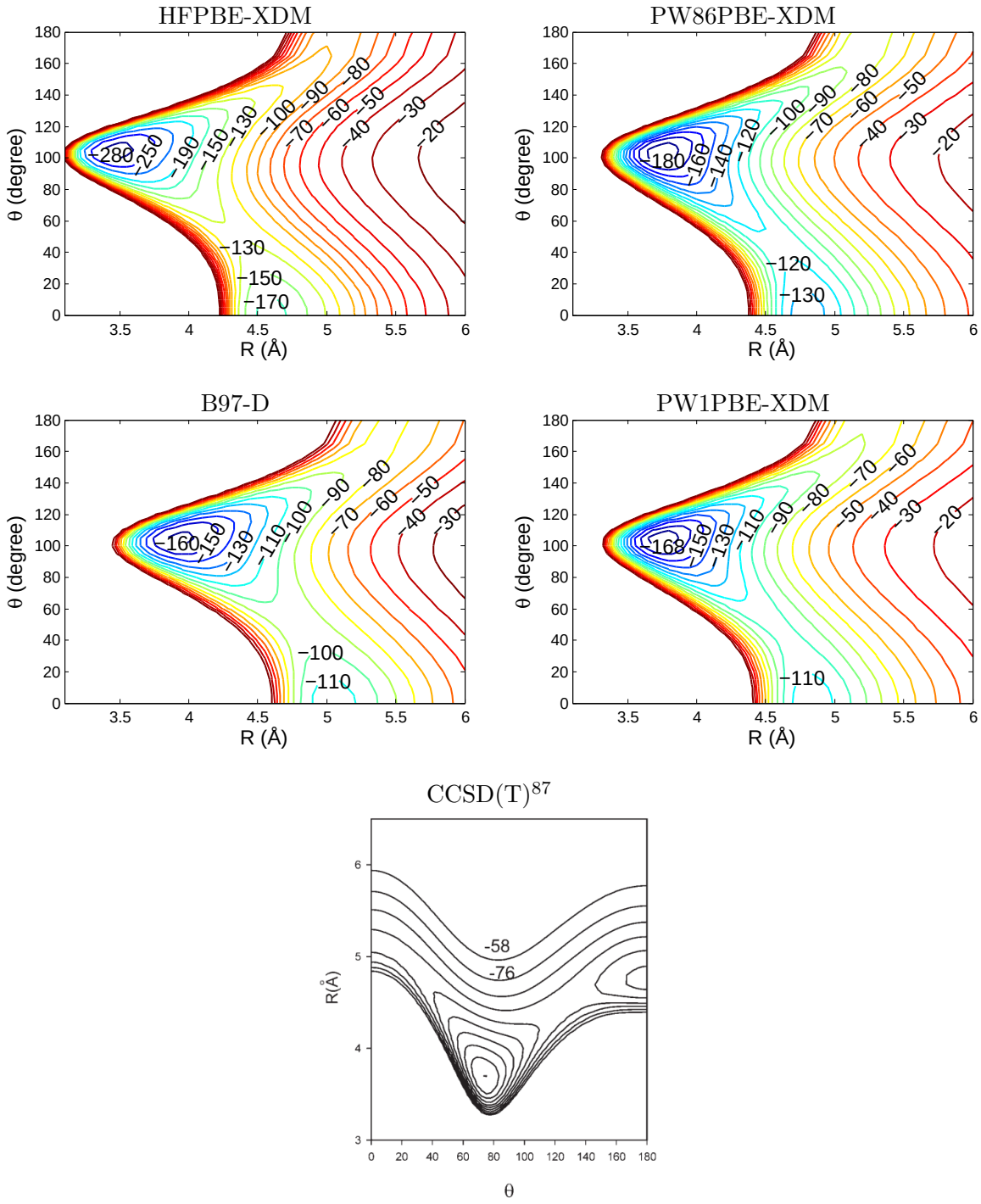

FIG. B.18. PES of Kr-OCS with XDM-corrected functionals and B97-D.

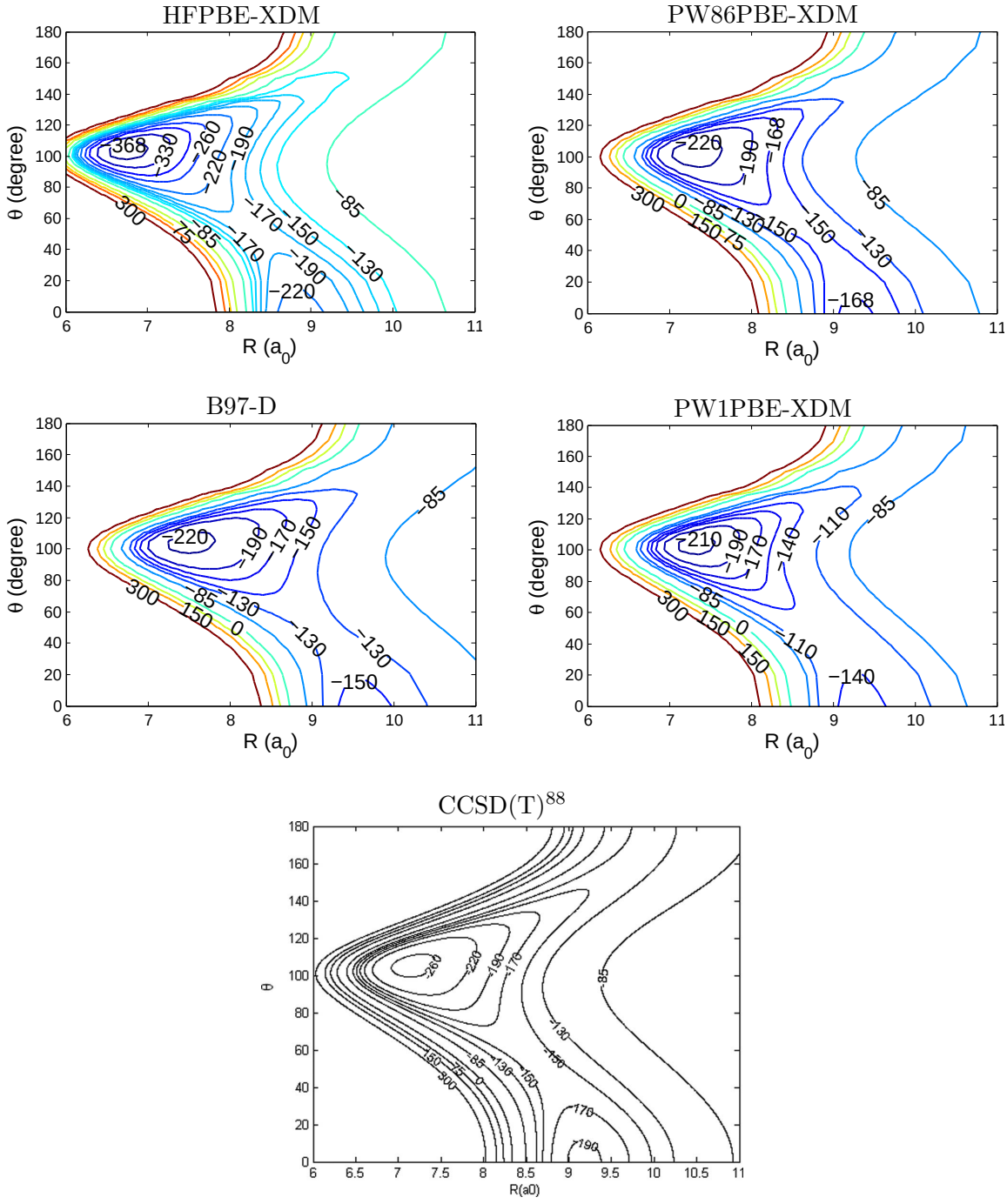

FIG. B.19. PES of He-HCN with XDM-corrected functionals and B97-D. The contours of the PES are in terms of milihartrees (mE_h).

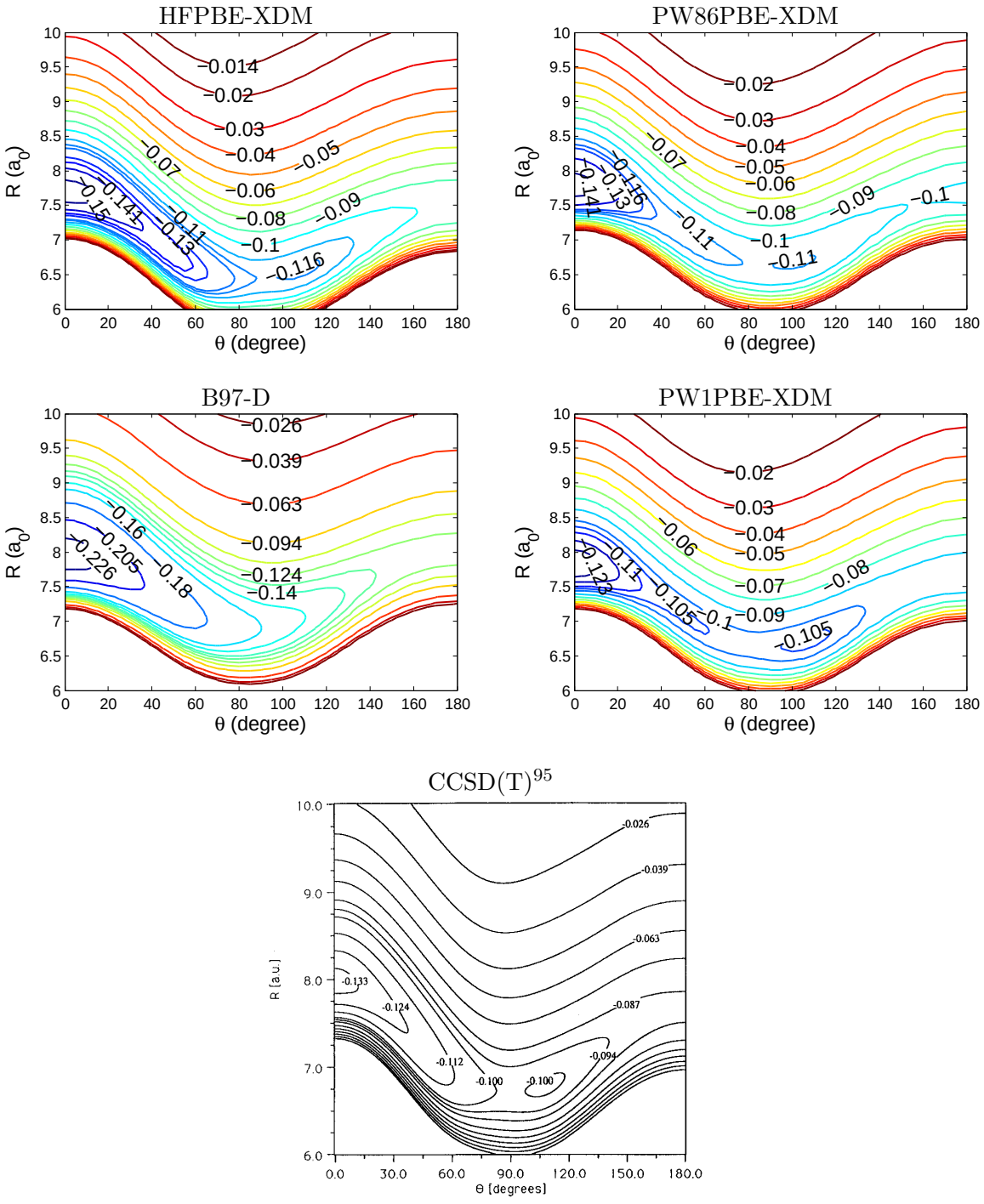

FIG. B.20. PES of Ne-HCN with XDM-corrected functionals and B97-D. The contours of the PES are in terms of milihartrees (mE_h).

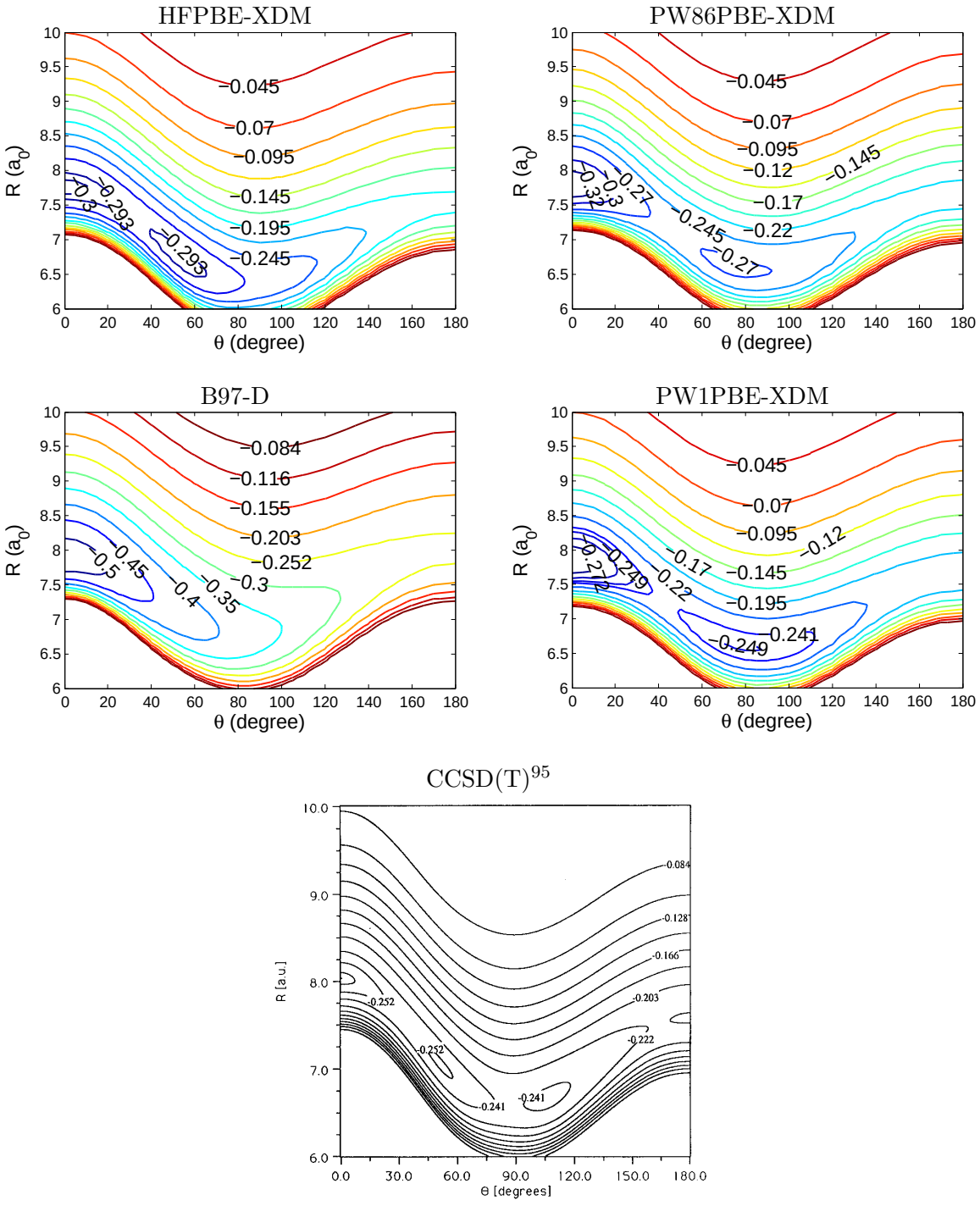

FIG. B.21. PES of Ar-HCN with XDM-corrected functionals and B97-D. The contours of the PES are in terms of milihartrees (mE_h).

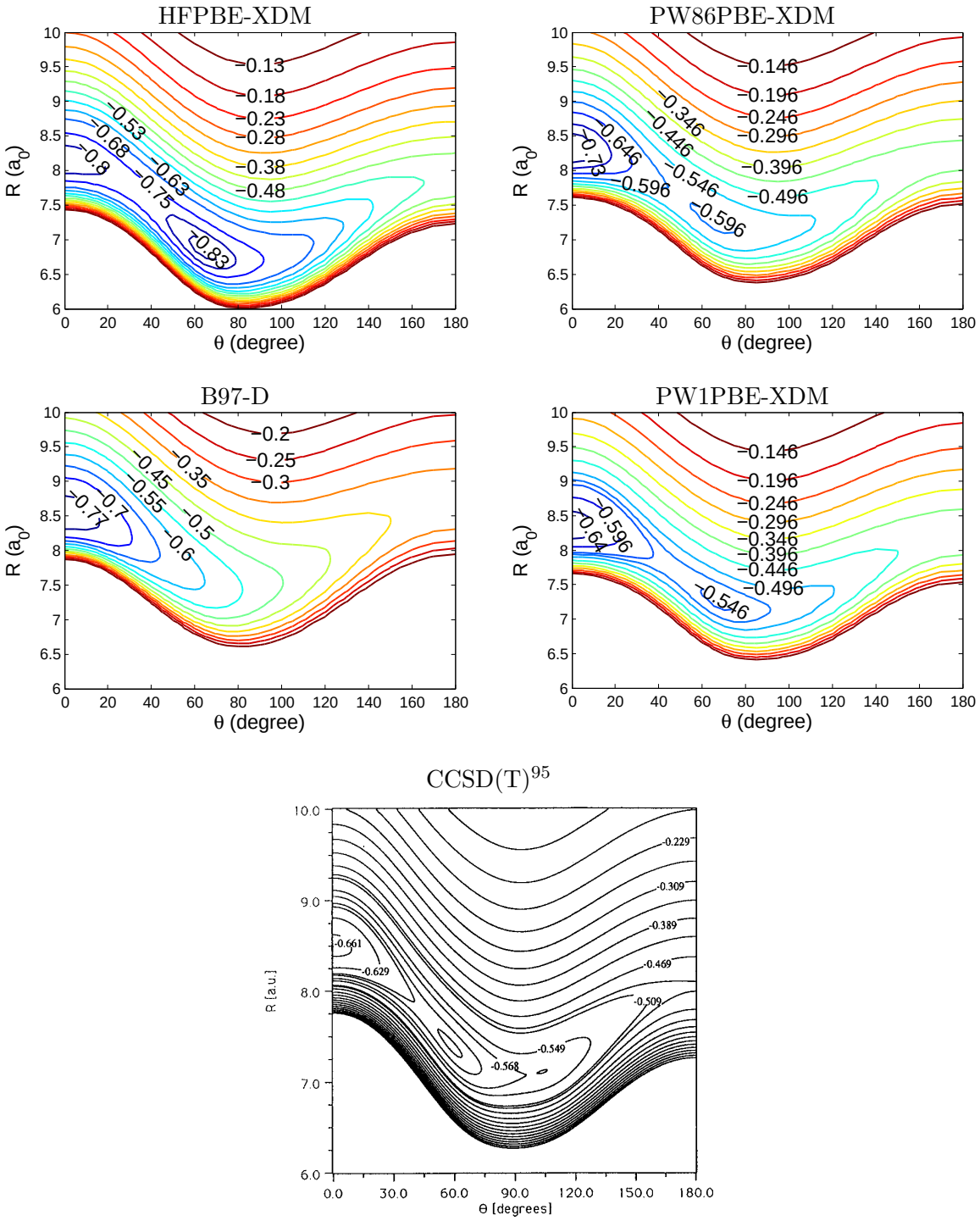

FIG. B.22. PES of Kr-HCN with XDM-corrected functionals and B97-D. The contours of the PES are in terms of milihartrees (mE_h).

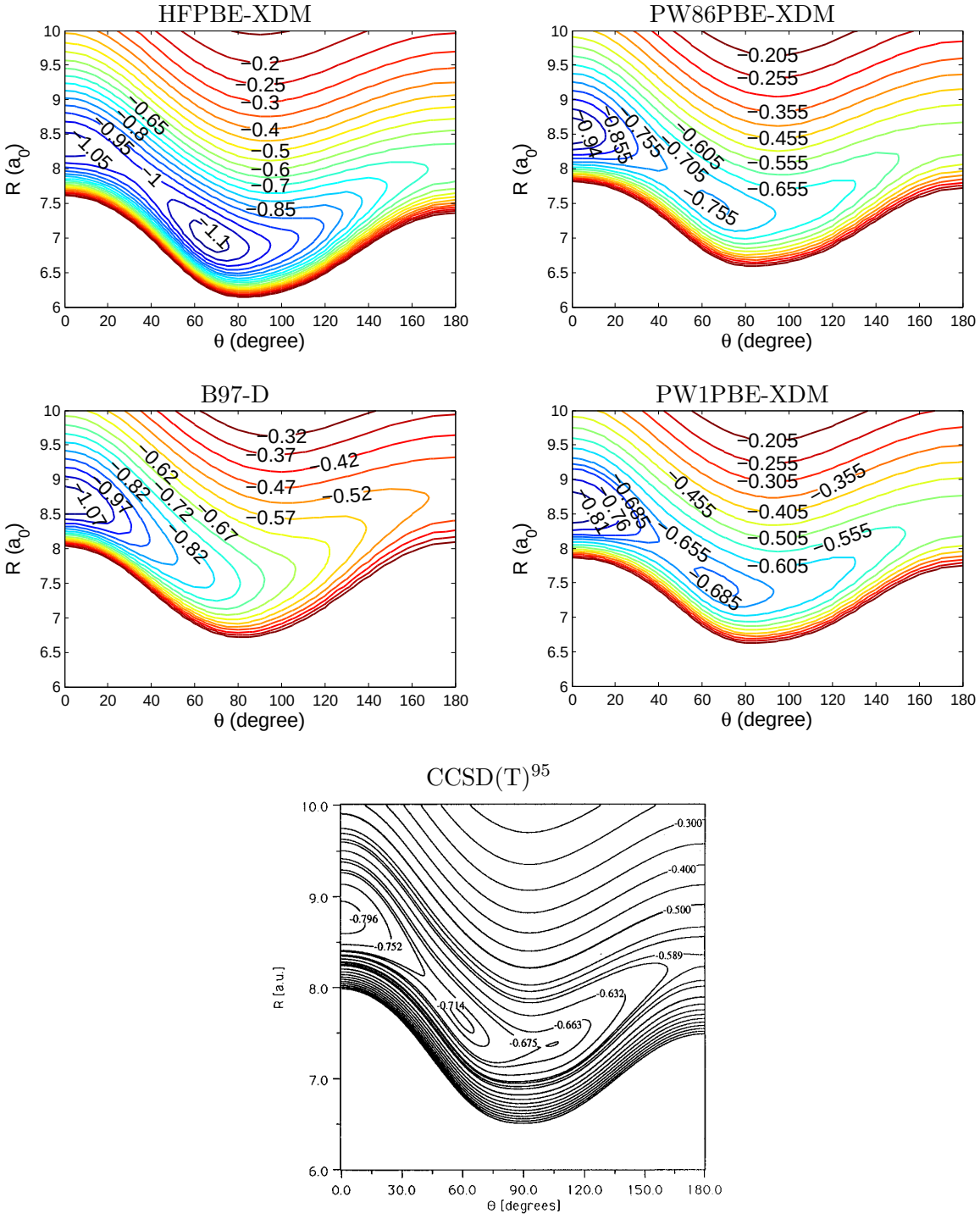

FIG. B.23. PES of He-C_2H_2 with XDM-corrected functionals and B97-D.

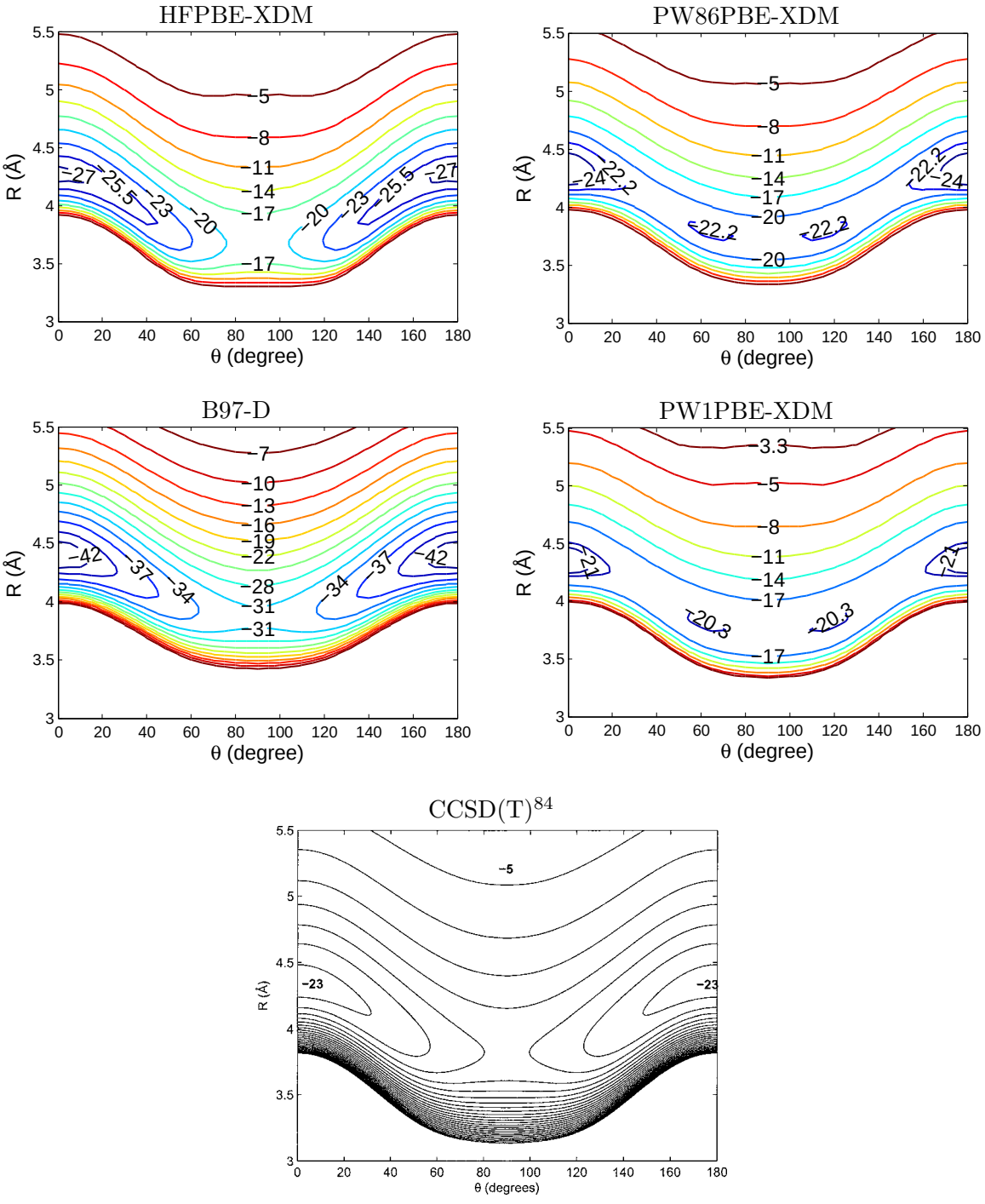

FIG. B.24. PES of Ne-C_2H_2 with XDM-corrected functionals and B97-D.

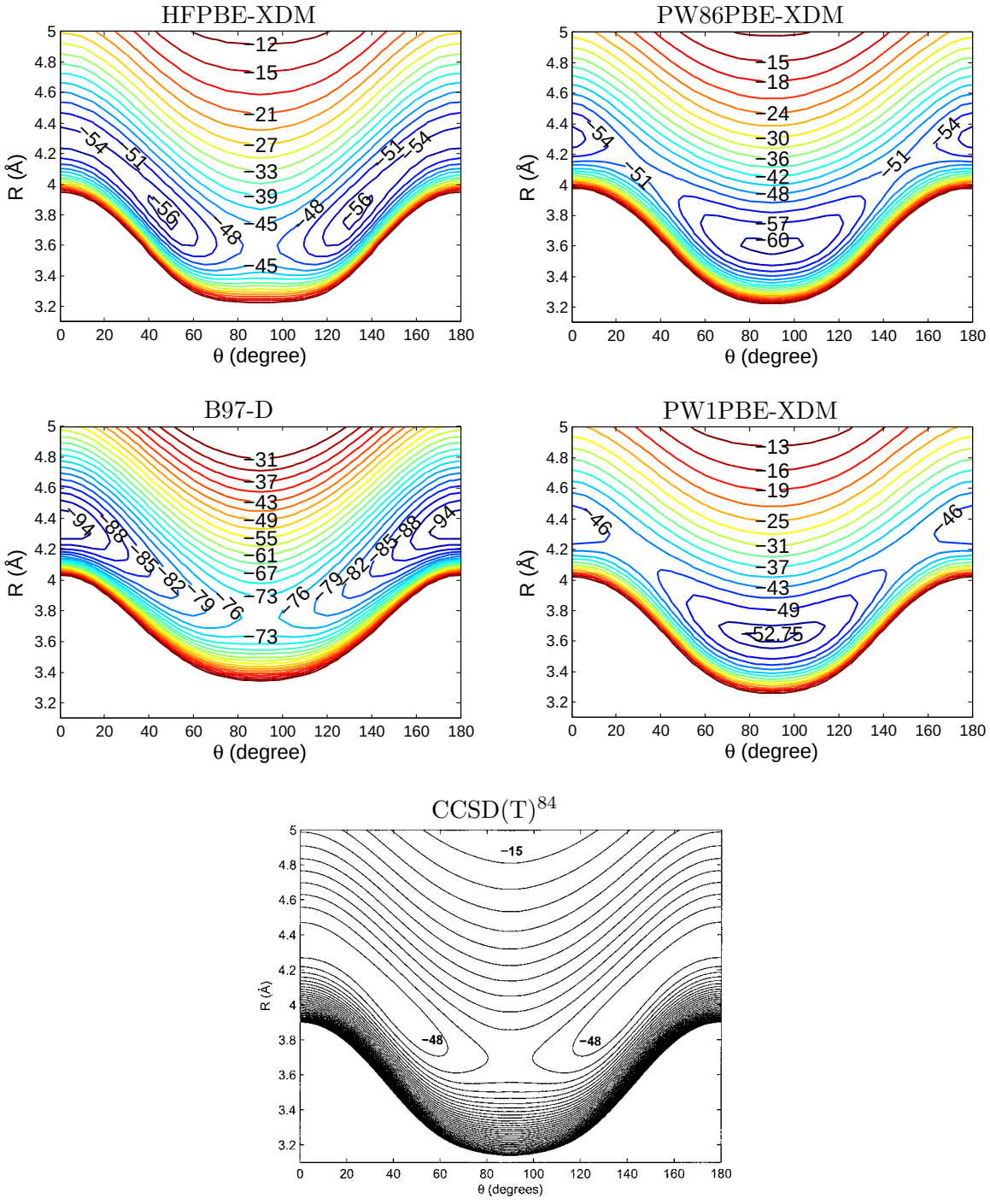

FIG. B.25. PES of Kr-C_2H_2 with XDM-corrected functionals and B97-D. The bond length is aligned at the horizontal axis of the reference PES.